Bull Earthquake Eng (2014) 12:517–547
DOI 10.1007/s10518-013-9537-1

ORIGINAL RESEARCH PAPER

Compatible ground-motion prediction equations for damping scaling factors and vertical-to-horizontal spectral amplitude ratios for the broader Europe region

S. Akkar · M. A. Sandıkkaya · B. Ö. Ay

Received: 29 January 2013 / Accepted: 9 October 2013 / Published online: 8 November 2013

Abstract In a companion article Akkar et al. (Bull Earthq Eng, doi:10.1007/s10518-013-9461-4, 2013a; Bull Earthq Eng, doi:10.1007/s10518-013-9508-6, 2013b) present a new ground-motion prediction equation (GMPE) for estimating 5 %-damped horizontal pseudo-acceleration spectral (PSA) ordinates for shallow active crustal regions in Europe and the Middle East. This study provides a supplementary viscous damping model to modify 5 %-damped horizontal spectral ordinates of Akkar et al. (Bull Earthq Eng, doi:10.1007/s10518-013-9461-4 2013a; Bull Earthq Eng, doi:10.1007/s10518-013-9508-6, 2013b) for damping ratios ranging from 1 to 50 %. The paper also presents another damping model for scaling 5 %-damped vertical spectral ordinates that can be estimated from the vertical-to-horizontal (V/H) spectral ratio GMPE that is also developed within the context of this study. For consistency in engineering applications, the horizontal and vertical damping models cover the same damping ratios as noted above. The article concludes by introducing period-dependent correlation coefficients to compute horizontal and vertical conditional mean spectra (Baker in J Struct Eng 137:322–331, 2011). The applicability range of the presented models is the same as of the horizontal GMPE proposed by Akkar et al. (Bull Earthq Eng, doi:10.1007/s10518-013-9461-4 2013a; Bull Earthq Eng, doi:10.1007/s10518-013-9508-6, 2013b): as for spectral periods 0.01 s $\leq$ T $\leq$ 4 s as

Electronic supplementary material The online version of this article (doi:10.1007/s10518-013-9537-1) contains supplementary material, which is available to authorized users.

S. Akkar (✉) · M. A. Sandıkkaya · B. Ö. Ay
Department of Civil Engineering, Earthquake Engineering Research Center,
Middle East Technical University, 06800 Ankara, Turkey
e-mail: sakkar@metu.edu.tr

M. A. Sandıkkaya
Institut des Sciences de la Terre (ISTerre), Universite de Grenoble,
38041 Grenoble, France

B. Ö. Ay
European Centre for Training and Research in Earthquake Engineering,
27100 Pavia, Italy

well as PGA and PGV for V/H model; and in terms of seismological estimator parameters $4 \leq M_w \leq 8$, $R \leq 200$ km, 150 m/s $\leq V_{S30} \leq 1{,}200$ m/s, for reverse, normal and strike-slip faults. The source-to-site distance measures that can be used in the computations are epicentral (R_{epi}), hypocentral (R_{hyp}) and Joyner–Boore (R_{JB}) distances. The implementation of the proposed GMPEs will facilitate site-specific adjustments of the spectral amplitudes predicted from probabilistic seismic hazard assessment in Europe and the Middle East region. They can also help expressing the site-specific design ground motion in several formats. The consistency of the proposed models together with the Akkar et al. (Bull Earthq Eng, doi:10.1007/s10518-013-9461-4 2013a; Bull Earthq Eng, doi:10.1007/s10518-013-9508-6, 2013b) GMPE may be advantageous for future modifications in the ground-motion definition in Eurocode 8 (CEN in Eurocode 8, Design of structures for earthquake resistance—part 1: general rules, seismic actions and rules for buildings. European Standard NF EN 1998-1, Brussels, 2004).

Keywords Damping scaling factors · Vertical-to-horizontal spectral amplitudes · Ground motion prediction equations for pan-European region · Conditional mean spectrum

1 Introduction

Base isolated structures, tall buildings and buildings with supplementary damping devices as well as the simplified equivalent linear procedures that mimic the nonlinear response of structures require scaling of commonly provided 5 %-damped response spectrum to different damping levels. In addition, the vertical seismic hazard becomes crucial especially for short-period critical structural facilities (e.g., nuclear power plants and dams) that are prone to structural damage upon the exceedance of a certain level of vertical displacement (Campbell and Bozorgnia 2003; Gülerce and Abrahamson 2011; Bommer et al. 2011). The vertical ground motions have also been identified as important for the design of lifeline systems and ordinary short-period structures in the vicinity of the fault (Elnashai and Papazoglu 1997; Kunnath et al. 2008; Gülerce and Abrahamson 2011). Thus, proper predictive models for describing vertical ground-motion demands and elastic spectral ordinates at different damping levels are always needed in the engineering community.

A detailed review on viscous damping scaling models for estimating spectral ordinates other than 5 % of critical is given in Rezaeian et al. (2012) and ATC (2010).[1] Currently, modern seismic design codes and guidelines suggest multiplicative factors to scale the 5 %-damped elastic spectral ordinates into ordinates for other damping ratios by period-independent tabulated values (e.g., NEHRP 2009)[1] or simple period-dependent expressions (e.g., Eurocode 8; CEN 2004). These simplified factors or expressions aggregate the likely influence of seismological parameters from a broad perspective. Consequently, their implementation to site-specific (or project-specific) probabilistic seismic hazard assessment (PSHA) may not always describe the accurate period-dependent variation of spectral ordinates for different damping levels.

The evolutionary progress in vertical design spectrum is summarized by Bommer et al. (2011) and Bozorgnia and Campbell (2004). Although it was common to use the ratio of 2/3 between vertical and horizontal design spectra in the past codes [based on the findings of Newmark and Hall (1982)], the recent seismic codes (e.g., NEHRP and Eurocode 8) acknowledge the period-dependent differences in the spectral shapes of horizontal and vertical design spec-

[1] ATC is Applied Technology Council and NEHRP is National Earthquake Hazards Reduction Program.

tra because the frequency content, magnitude- and distance-dependent scaling of horizontal and vertical ground motions differ. The aforementioned codes define simplified vertical-to-horizontal (V/H) spectral ratios that are conditioned on PGA (Eurocode 8) and PSA at T = 0.2 s (NEHRP). Though conceptually different, the period-dependent V/H spectral ratios defined by these codes consider magnitude and source-to-site distance effects on vertical design spectrum. The NEHRP provisions also consider the influence of site class on the V/H ratios whereas differences in site class are assumed to be insignificant in Eurocode 8. For practical reasons, the above described generic V/H ratios can be of use for defining vertical code-based spectrum. However, such oversimplified expressions are not appropriate for site-specific probabilistic hazard studies. PSHA requires consistent and compatible earthquake scenarios for horizontal and vertical ground motions that are determined through scenario spectrum (computed from deaggregation of hazard at a specific period) or conditional mean spectrum, CMS (Baker 2011). [The reader is referred to Gülerce and Abrahamson (2011) for extended discussions on the implementation of V/H GMPEs to scenario spectrum and CMS]. This point is even more important if vertical and horizontal acceleration time series have to be selected and scaled for the target hazard levels. For such cases, empirical V/H spectral ratio models are required for a proper mapping of source, path and site effects on to V/H ratios. Moreover, such complete V/H GMPEs would be beneficial for further improvements in code-based generic V/H spectral ratio expressions.

This paper describes a set of ground-motion predictive models for scaling 5 %-damped horizontal and vertical spectral ordinates for viscous damping ratios varying between 1 and 50 %. The chosen damping range can sufficiently address the needs of most seismic design and performance assessment projects. The paper also describes a model for predicting the ratios of vertical-to-horizontal 5 %-damped PSA ordinates. These predictive models are derived from the ground-motion database used by Akkar et al. (2013a,b) that developed a GMPE for horizontal PSA for its use in the seismic hazard assessment of shallow active crustal regions in Europe and the Middle East. Having been developed from the same pan-European ground-motion database with the same spectral period interval and capable of addressing different distance metrics, the predictive models presented in this paper are the first fully compatible GMPEs for producing consistent scenario-based horizontal and vertical design spectra at different damping levels that can be of use in many engineering applications in the broader Europe region. The applicability range of the proposed models in this paper is similar to the horizontal Akkar et al. (2013a,b) GMPE. This property can be useful in future studies to update the definitions of horizontal and vertical ground-motion demands in Eurocode 8 (CEN 2004). The paper also introduces the epsilon-based correlation coefficients that are used for developing horizontal and vertical conditional mean spectra (CMS); a concept proposed by Baker (2011) that accounts for the period-dependent variability of ground motion for scenario spectrum. The proposed models, together with the horizontal Akkar et al. (2013a,b) GMPE can also be used in vector-valued PSHA (Bazzurro and Cornell 2002) in Europe and surrounding regions.

2 Strong-motion database

The strong-motion accelerograms used in this study are selected from RESORCE (Akkar et al. 2013c). RESORCE is developed for the **S**e**I**smic **G**round **M**otion **A**ssessment (SIGMA; http://projet-sigma.com/index.html) project and it is the updated and extended version of the pan-European databases compiled under the **S**eismic **H**azard H**AR**monization in **E**urope (SHARE) project (Yenier et al. 2010). The database consists of 1,041 accelerograms recorded

from 221 shallow active crustal earthquakes. The epicentral locations of most of these events cover the Mediterranean region and the Middle East. The moment magnitudes (M_w) of recordings range between 4 and 7.6 and their source-to-site distances (R_{JB}; closest distance between the vertical projection of ruptured fault and site) are up to 200 km. The strong-motion records in the database have the complete information on epicentral (R_{epi}) and hypocentral (R_{hyp}) distances as well. The site conditions of all accelerograms are identified by measured V_{S30} (time based average shear-wave velocity of the upper 30 m soil layer). The V_{S30} interval of the database is between 92 and 2,165 m/s. The database consists of normal, reverse and strike-slip earthquakes of focal depths less than 30 km. Only three-component accelerograms recorded at free-field stations are used. Singly recorded events are removed from the database. The reader is referred to Akkar et al. (2013a,b) for the overall and specific features of the strong-motion database as it is common for both studies.

The horizontal and vertical PSA at 16 different damping levels (i.e., 1, 2, 3, 4, 5, 6, 7, 8, 9, 10, 15, 20, 25, 30, 40 and 50 %) are computed from the compiled strong-motion database to develop the GMPEs for damping scaling and V/H spectral ratios. The dense damping distribution towards lower damping levels is a modeling requirement for a better fit on the observed data. The geometric means of horizontal PGA, PGV and 62 spectral ordinates ($0.01\ s \leq T \leq 4.0\ s$) represent the horizontal ground-motion demands in the proposed GMPEs. The selected spectral periods are the same as those used in Akkar et al. (2013a,b). This way full compatibility is provided between the models developed here and the GMPE for the horizontal PSA presented in Akkar et al. (2013a,b). The usable spectral period band of each accelerogram is computed by using the criteria set in Akkar and Bommer (2006).

3 Predictive equations for damping scaling factors

Bommer and Mendis (2005), Lin et al. (2005) and Rezaeian et al. (2012) give a detailed literature review on the predictive models for damping scaling factor (DSF). As shown in Eq. (1), DSF is the normalized PSA of different damping levels (β) with PSA at 5 % damping.

$$DSF = \frac{\text{PSA at } \beta\% \text{ damping}}{\text{PSA at } 5\% \text{ damping}} \tag{1}$$

Most of the previous DSF models are either built on β (e.g., Ashour 1987; Tolis and Faccioli 1999; Priestly 2003; NEHRP) or β together with spectral period, T, (e.g., Newmark and Hall 1982; Wu and Hanson 1989; Idriss 1993; Naeim and Kircher 2001; Ramirez et al. 2000, 2002; Lin and Chang 2003; Atkinson and Pierre 2004; Malhotra 2006; Eurocode 8). Few models discussed the effects of other independent parameters on DSF. Stafford et al. (2008) emphasized the significance of duration whereas Abrahamson and Silva (1996) included M_w as an additional predictor variable in their model. Lin and Chang (2004) and Hatzigeorgiou (2010) indicated the role of site class on DSF and considered this parameter in their functional forms. Cameron and Green (2007) modeled the influence of tectonic regime in their damping scaling relationship together with other important estimator parameters such as M_w, site class and source-to-site distance. The most recent study conducted by Rezaeian et al. (2012) showed that magnitude, source-to-site distance and spectral period are sufficient for unbiased DSF estimates.

In this study, the natural logarithm of DSF is regressed against M_w, R_{JB}, SoF (style-of-faulting) and V_{S30} for each damping level and period. Other estimator parameters (e.g., duration) are not included to keep the model as simple as possible for lesser complexity in hazard studies. The Akkar et al. (2013a,b) functional form is chosen as the backbone

expression for the DSF model. The magnitude scaling in Akkar et al. (2013a,b) is quadratic with a break in the linear term whereas a magnitude-dependent geometrical spreading is considered to account for path effects. The site term in Akkar et al. (2013a,b) is composed of linear and nonlinear terms for a realistic modeling of soil behavior. Akkar et al. (2013a,b) address the SoF effects on ground-motion amplitudes by dummy variables for normal and reverse events over strike-slip earthquakes. The preliminary regression results showed that the bilinear magnitude scaling function or consideration of higher order magnitude terms in the backbone functional form do not increase the accuracy of DSF estimates. The magnitude-dependent slope term in geometrical spreading also did not play an efficient role on the distance scaling of median DSF trends. None of these complicated functions in magnitude and distance scaling decreased the standard deviation (aleatory variability) of the model. The style-of-faulting effect is also disregarded in the final model as DSF is insensitive to different faulting mechanisms. The averages of residual distributions for each SoF are almost zero that also justifies the decision to disregard the SoF terms in the final DSF model. It should be noted that the non-uniform SoF distribution in the strong-motion database may mask the actual effect of this parameter on DSF. Thus, overlooking the SoF effect in the DSF predictive model can increase the epistemic uncertainty in our DSF estimates. The fictitious depth term in distance scaling is also kept constant for all spectral periods to have a smooth variation in the spectral shape. Consideration of fictitious depth as a period-dependent parameter did not change the model estimates, which advocates its marginal effect on DSF estimates. The nonlinear site amplification term is dropped after the first round of regression analyses as the variation of DSF is independent of nonlinear soil behavior. Thus, the modification of DSF amplitudes due to different soil conditions is described by the linear site term. The linear site term is constrained to a constant value for $V_{S30} > 1{,}000$ m/s. The V_{S30} for reference rock condition is defined as $V_{REF} = 750$ m/s in the site term. The final functional form of the DSF ground-motion model is given in Eq. (2).

$$\ln(DSF) = c_1 + c_2(M_w - 6.75) + c_3 \ln\left(\sqrt{R_{JB}^2 + c_5^2}\right) + c_4 \ln\left[\frac{\min(V_{S30}, 1,000)}{V_{REF}}\right] \quad (2)$$

In the above expression, c_i (i = 1–4) denotes period-dependent regression coefficients computed by mixed-effects regression procedure (Abrahamson and Youngs 1992). They are smoothed by moving average technique to prevent jagged DSF trends. The regression coefficient c_5 is the fictitious depth term and it is taken as constant ($c_5 = 5$) for the entire period range for horizontal and vertical DSF models. The previous models for DSF (e.g., Trifunac and Lee 1989; Boore et al. 1993; Bommer et al. 1998; Berge-Thierry et al. 2003; Faccioli et al. 2004; Akkar and Bommer 2007) provide different sets of regression coefficients for each damping level. This approach is not followed in this study. Each regression coefficient c_i (i = 1–4) is represented by a quadratic function in terms of natural logarithm of β (in percent) as given in Eq. (3).

$$c_i = b_{i1} + b_{i2} \ln(\beta/5) + b_{i3} [\ln(\beta/5)]^2 \quad (3)$$

The primary aim of this approach is to increase the applicability of the model. Newmark and Hall (1982) are the first proponents of such polynomial functions. In their paper, Newmark and Hall (1982) proposed a linear function. We tried polynomial functions of different orders. The observations from these trials indicated that the quadratic function (Eq. 3) is sufficient to explain the data trend. Rezaeian et al. (2012) also use a quadratic expression in their damping model. Figure 1 compares the performance of Eq. (3) with the discrete DSF estimates that are directly obtained from regressions on Eq. (2). The comparisons are done for different damping levels and for a strike-slip earthquake scenario of M_w 7.5. The rock site (V_{S30} =

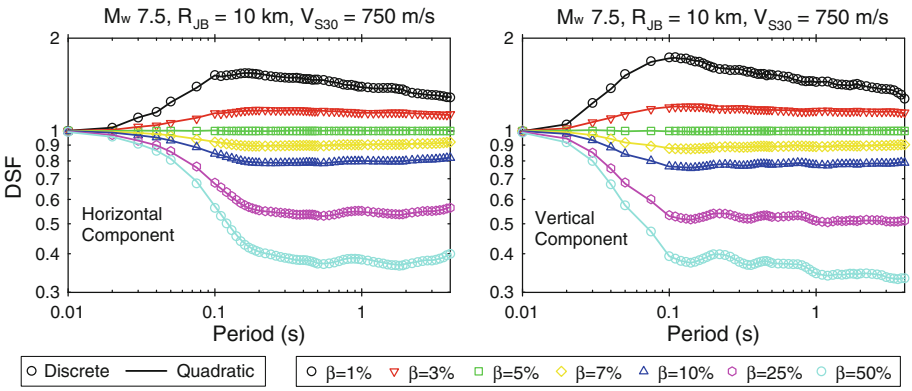

Fig. 1 Discrete damping scaling factors obtained from direct regressions on Eq. (2) for each damping level and their comparisons with those computed from Eq. (3) that describes each regression coefficient in Eq. (2) as a quadratic function

750 m/s) is located at a distance of R_{JB} = 10 km from the causative fault. The left and right panels show the comparisons for horizontal and vertical spectral components, respectively. The patterns between the comparative plots overlap with each other that certify the success of Eq. (3) in representing the regression coefficients c_i (i = 1 − 4) to estimate DSFs for different damping values. The rational functional form of Bommer et al. (1998) that is used in Eurocode 8 was also evaluated as an alternative to Eq. (3) while developing the proposed DSF model. However, it was discarded in the later stages of the study because the resultant DSF estimates were unrealistic. Table 1 presents the horizontal spectral ordinate DSF regression coefficients b_{ij} for each c_i for a set of selected spectral periods. The index i varies from 1 to 4 whereas j takes values between 1 and 3. In a similar way, Table 2 lists the same regression coefficients for the DSF model of vertical spectral ordinates.

The within-event (ϕ) and between-event (τ) standard deviations are computed by using quadratic expressions that are given in Eq. (4). The total standard deviation (σ) is the square root of the sum of the squares of within-event and between-event standard deviation terms. The regression coefficients of within- and between-event standard deviations for horizontal and vertical DSF models are given in Tables 3 and 4, respectively for the periods listed in Tables 1 and 2. The model regression coefficients for the full list of spectral ordinates are available in the electronic supplement to this article.

$$\phi = b_{61} + b_{62}\ln(\beta/5) + b_{63}[\ln(\beta/5)]^2 \tag{4a}$$

$$\tau = b_{71} + b_{72}\ln(\beta/5) + b_{73}[\ln(\beta/5)]^2 \tag{4b}$$

$$\sigma = \sqrt{\phi^2 + \tau^2} \tag{4c}$$

Figure 2 shows the magnitude, distance and V_{S30} dependent variations of the proposed DSF model for horizontal (left column) and vertical (right column) PSA ordinates at T= 0.1 s. The effect of damping is prominent at short spectral periods, which is the main reason for choosing T = 0.1s in this illustrative case. The effect of magnitude scaling on DSF is presented on the 1st row for a stiff site (V_{S30} = 525 m/s) located at a distance of R_{JB} = 15 km from the causative fault. The magnitude influence is more visible on horizontal ground motions when β attains larger values. The variations in DSF for vertical spectral ordinates are less sensitive to magnitude. However, as in the case of horizontal DSF model, magnitude effect starts contributing to vertical DSF variations for heavily damped structural systems (i.e.,

Table 1 DSF regression coefficients for horizontal spectral ordinates

Period (s)	b_{11}	b_{12}	b_{13}	b_{21}	b_{22}	b_{23}	b_{31}	b_{32}	b_{33}	b_{41}	b_{42}	b_{43}
0.01	0.001198	−0.00358	−0.00124	0.00004	0.000045	0.000595	−0.00032	0.000585	0.00005	−0.0001	0.001432	−0.00111
0.02	0.001663	−0.03478	−0.00165	−0.00042	0.000684	0.000079	−0.00032	0.007236	0.00023	0.000387	−0.00046	−0.00059
0.03	0.005268	−0.10669	0.006535	−0.00041	0.002418	0.001401	−0.00093	0.021327	−0.00128	0.000664	−0.01002	−0.00047
0.04	0.003168	−0.16643	0.005757	−0.00068	0.014843	0.00156	−0.00015	0.032546	−0.00059	0.00105	−0.02782	0.000878
0.05	0.001719	−0.23363	0.00509	−0.00017	0.019448	0.005037	0.000518	0.043221	0.000537	0.001386	−0.0365	$-8.2E-05$
0.075	−0.00246	−0.33204	−0.00979	−0.00025	0.031044	0.008748	0.001643	0.051293	0.005062	0.00189	−0.04572	−0.00212
0.10	0.001867	−0.37117	−0.03101	0.000455	0.028815	0.011975	0.000706	0.040656	0.010132	0.001147	−0.07169	−0.00393
0.15	−0.00138	−0.38038	−0.06364	−0.00135	0.022613	0.011994	0.00053	0.025346	0.013599	−0.00053	−0.05921	−0.01104
0.20	0.001431	−0.33998	−0.06977	−0.00175	0.014247	0.011454	−0.00042	0.005123	0.011979	0.002233	−0.03628	−0.01206
0.30	0.005664	−0.28422	−0.06911	−0.00202	0.002101	0.009863	−0.00115	−0.01348	0.008246	0.000096	−0.01385	−0.01315
0.40	0.008775	−0.247	−0.06433	−0.00203	−0.00671	0.006677	−0.00158	−0.02594	0.005468	0.001794	−0.00354	−0.007
0.50	0.005547	−0.23394	−0.06448	−0.00209	−0.01892	0.003051	−0.0008	−0.02792	0.005283	−0.0009	0.015135	−0.00043
0.75	0.008193	−0.1923	−0.05717	−0.00095	−0.02443	−0.00206	−0.00122	−0.0358	0.002565	0.000301	0.039576	0.004235
1.00	0.00392	−0.17601	−0.04841	−0.00052	−0.03092	−0.00581	−0.0003	−0.03733	−0.00061	−0.00112	0.044602	0.00561
1.50	0.004771	−0.16221	−0.04924	0.000871	−0.04225	−0.01033	−0.00037	−0.04071	−0.00146	−0.00024	0.036168	0.003788
2.00	0.007292	−0.1398	−0.05212	0.000892	−0.04892	−0.01261	−0.00091	−0.04492	−0.00108	−0.00017	0.016833	0.001299
3.00	0.005723	−0.11785	−0.0493	0.001401	−0.05677	−0.01428	−0.00061	−0.04518	−0.00246	−0.00018	0.004307	−0.00283
4.00	0.011176	−0.10534	−0.04561	0.002951	−0.06213	−0.01519	−0.00186	−0.04301	−0.00308	0.002149	0.01449	0.000704

Table 2 DSF regression coefficients for vertical spectral ordinates

Period (s)	b_{11}	b_{12}	b_{13}	b_{21}	b_{22}	b_{23}	b_{31}	b_{32}	b_{33}	b_{41}	b_{42}	b_{43}
0.01	0.002398	−0.00464	−0.00233	0.000134	0.000824	0.000178	−0.00054	0.001026	0.000096	−0.00034	0.001767	−0.00042
0.02	0.005533	−0.06364	−0.00289	−0.00043	0.000809	−0.00031	−0.00111	0.012461	0.000398	0.000423	−0.00315	−0.00015
0.03	0.010098	−0.21702	0.006742	0.000278	0.002155	0.001846	−0.0016	0.041863	−0.00077	0.000357	−0.01709	0.001313
0.04	0.005007	−0.34911	$-8.2E-05$	0.000571	0.008769	0.002005	−0.00098	0.06518	0.00136	−0.00392	−0.02208	0.000569
0.05	−0.0058	−0.4374	−0.00941	−0.00086	0.006867	0.002161	0.001963	0.075147	0.005143	−0.0016	−0.02277	0.006149
0.075	−0.00277	−0.48161	−0.03847	0.000331	0.009436	0.008139	0.001848	0.063017	0.012584	0.002601	−0.01395	0.000355
0.10	−0.00546	−0.5014	−0.05565	−0.00024	0.005231	0.008305	0.001058	0.054456	0.013547	−0.00459	−0.01566	−0.00549
0.15	−0.00232	−0.43125	−0.06884	−0.0023	0.004934	0.011808	−0.0004	0.025253	0.014911	−0.00146	−0.01647	−0.00384
0.20	0.000263	−0.36461	−0.06749	−0.00213	0.011499	0.013214	−0.00065	0.006098	0.013541	−0.0021	−0.00182	−0.0047
0.30	0.003355	−0.33041	−0.06519	−0.00165	−0.00078	0.010869	−0.00156	−0.00524	0.009268	−0.00119	0.003087	−0.00831
0.40	0.003602	−0.29517	−0.06264	−0.00109	−0.00217	0.007274	−0.00026	−0.014	0.006229	0.001091	0.010125	−0.0098
0.50	0.00246	−0.27448	−0.05932	−0.00258	−0.00901	0.005028	−0.00064	−0.0204	0.0055	−0.00021	0.02152	−0.00359
0.75	0.001086	−0.25524	−0.05557	0.000542	−0.01312	−0.00124	0.000952	−0.02097	0.002209	0.000718	0.031537	0.00227
1.00	0.001147	−0.23412	−0.05651	−0.00035	−0.02405	−0.00721	−0.00027	−0.02944	0.000776	−0.00256	0.017635	0.006128
1.50	0.005222	−0.21514	−0.06118	0.00074	−0.03342	−0.01028	−0.00088	−0.03177	0.001425	−0.00172	0.02434	0.00653
2.00	0.002785	−0.20364	−0.05809	0.001242	−0.04422	−0.01025	−0.00032	−0.03204	0.000413	−0.0018	0.017399	0.003592
3.00	0.006202	−0.19389	−0.06675	0.001639	−0.05576	−0.01244	−0.00054	−0.03002	0.001253	0.000168	−0.00426	−0.00249
4.00	0.009549	−0.16484	−0.0776	0.001935	−0.06004	−0.01763	−0.00185	−0.03143	0.002593	−0.00107	−0.0094	−0.00754

Table 3 Standard deviation regression coefficients of the DSF model for horizontal spectral ordinates

Period (s)	b_{61}	b_{62}	b_{63}	b_{71}	b_{72}	b_{73}
0.01	0.005265	0.000924	0.005494	0.003564	−0.00135	0.002088
0.02	0.014935	−0.00456	0.013462	0.005076	−0.00226	0.003633
0.03	0.035034	−0.00757	0.028221	0.008231	−0.00048	0.009057
0.04	0.052255	−0.00348	0.039481	0.015437	−0.00198	0.01255
0.05	0.058578	−0.00406	0.044772	0.010115	0.000274	0.013369
0.075	0.068836	0.000203	0.050315	0.011068	0.005923	0.016025
0.10	0.065102	0.001334	0.050329	0.015893	0.000911	0.018006
0.15	0.062401	0.004246	0.049681	0.00669	0.004142	0.011661
0.20	0.064469	0.004089	0.046537	0.006733	0.004407	0.011793
0.30	0.061431	0.004647	0.045281	0.008272	0.000026	0.012741
0.40	0.062847	0.005084	0.044374	0.005145	0.000695	0.013102
0.50	0.058855	0.002856	0.044091	0.012835	0.002618	0.016743
0.75	0.064181	0.006075	0.044561	0.008911	−0.00132	0.013721
1.00	0.063034	0.005479	0.045448	0.016261	0.001629	0.015567
1.50	0.06232	0.002838	0.04653	0.012108	0.009527	0.017909
2.00	0.058796	0.008895	0.046878	0.008415	0.004801	0.01597
3.00	0.052093	0.011071	0.042998	0.01788	0.006693	0.022389
4.00	0.047785	0.014943	0.041903	0.0197	0.015215	0.021287

Table 4 Standard deviation regression coefficients of the DSF model for vertical spectral ordinates

Period (s)	b_{61}	b_{62}	b_{63}	b_{71}	b_{72}	b_{73}
0.01	0.002946	−0.0008	0.002973	0.001733	−0.00104	0.001661
0.02	0.009187	−0.00222	0.008102	0.002404	−0.00088	0.002426
0.03	0.017113	−0.0047	0.016379	0.005133	−0.00051	0.00511
0.04	0.025923	−0.00359	0.022437	0.011986	−0.00225	0.010168
0.05	0.034072	−0.0022	0.029385	0.013388	0.002185	0.013223
0.075	0.049981	0.000757	0.041528	0.015192	0.003326	0.018309
0.10	0.049716	0.002192	0.042586	0.018613	0.008826	0.020338
0.15	0.051899	0.007075	0.047045	0.013493	0.007444	0.015328
0.20	0.04933	0.00793	0.043589	0.009903	0.01014	0.012507
0.30	0.048411	0.005822	0.040023	0.000065	0.000723	0.012317
0.40	0.047006	0.008451	0.038979	0.006417	0.001097	0.012472
0.50	0.046804	0.005188	0.037081	0.00964	0.001451	0.011667
0.75	0.046953	0.007885	0.038768	0.012584	0.001159	0.015274
1.00	0.049176	0.006004	0.040136	0.00439	0.006055	0.012511
1.50	0.047777	0.009043	0.042481	0.013316	0.006169	0.016945
2.00	0.046394	0.011464	0.040939	0.01072	0.006785	0.015758
3.00	0.043665	0.010874	0.038291	0.014682	0.013664	0.020779
4.00	0.040025	0.014647	0.036967	0.017957	0.015872	0.02218

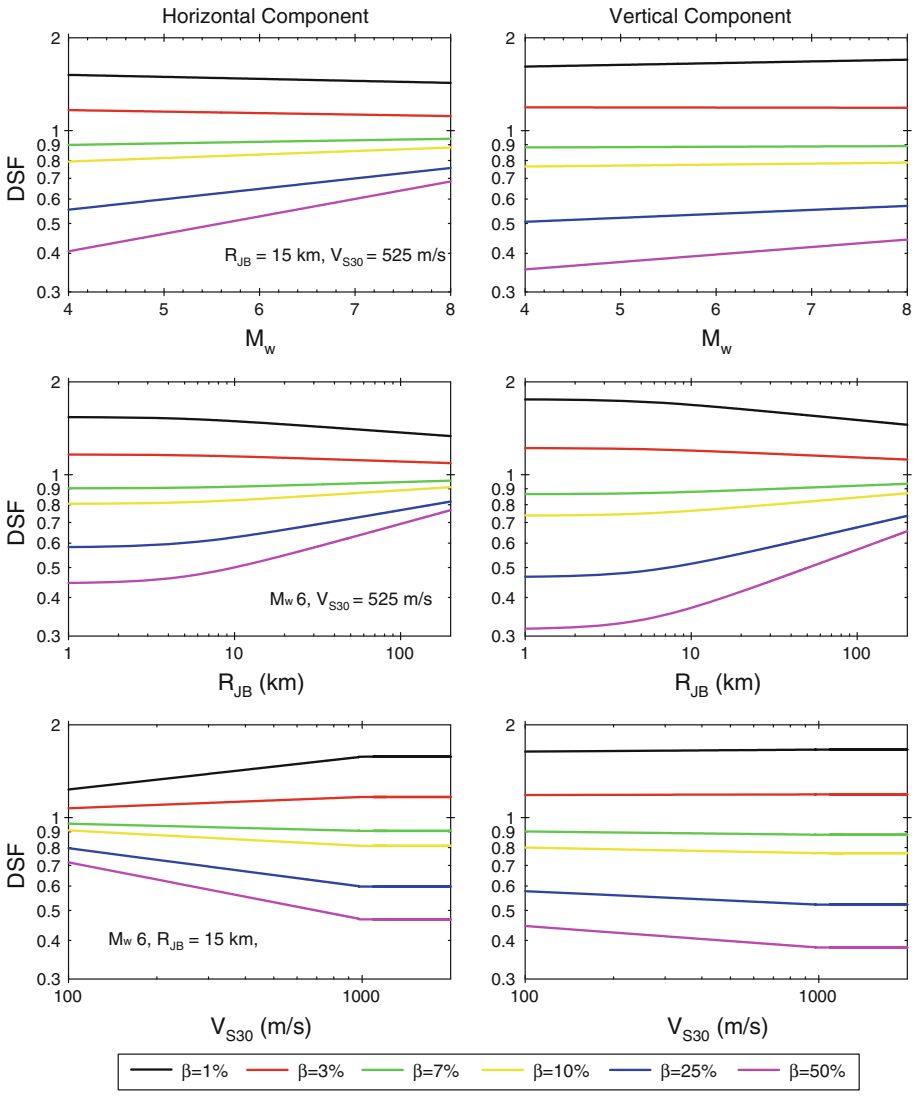

Fig. 2 Magnitude (*first row*), distance (*second row*) and V_{S30} (*third row*) dependent variation of horizontal (*left panel*) and vertical (*right panel*) DSF at T = 0.1s

$\beta \geq 20\,\%$). Distance-dependent scaling of DSF is plotted in the 2nd row on Figure 2 for M_w 6 and $V_{S30} = 525$ m/s. The effect of distance on DSF seems to be more apparent than the influence of magnitude. The decay due to geometrical spreading of DSF is faster at very low ($\beta < 3\,\%$) and high ($\beta > 15\,\%$) damping ratios. The 3rd row plots on Figure 2 shows the V_{S30} scaling of DSF for a scenario event of M_w 6 and $R_{JB} = 15$ km. The damping scaling of horizontal ground motions grows with increasing V_{S30} up to 1,000 m/s and becomes stable after $V_{S30} = 1{,}000$ m/s (imposed by the site model). This trend is more visible at lower and higher damping ratios. As in the case of magnitude, the damping scaling of vertical spectrum becomes sensitive to the changes in V_{S30} when β attains larger values (i.e., $\beta \geq 20\,\%$).

Figure 3 compares the horizontal (top row) and vertical (bottom row) DSF models with those of Rezaeian et al. (2012) and Eurocode 8 (CEN 2004). The Rezaeian et al. (2012) model is abbreviated as Retal12 on the plots. The comparisons are made for two different magnitudes: M_w 4.5 (left column) and M_w 7.5 (right column) that resemble low seismicity (Type II) and high seismicity (Type I) regions, respectively according to Eurocode 8. The fictitious site is selected as a generic rock site with $V_{S30} = 800$ m/s. It is located at a distance of $R_{JB} = 10$ km from a 90 degrees dipping strike-slip fault. The top of the ruptured fault segment is assumed to be 5 km below the surface for both cases. Under this simple source geometry the corresponding rupture distance (R_{rup}; the distance measure used in the Retal12) is computed as 11.2 km. The comparative plots indicate that DSF estimates of this study and Retal12 agree with each other fairly well. There are differences in the DSF values of Eurocode 8 and the other two GMPEs. The Eurocode 8 damping scaling is sensitive to period variation only in the very short spectral period range. The other two DSF models consider the period influence on damping for the entire period band. This conceptual difference between Eurocode 8 and the other two DSF models show itself particularly in low seismicity regions (mimicked by M_w 4.5), towards longer periods ($T > 1.0$ s) and when β attains large values. For short-period spectral regions, the two DSF models tend to estimate larger spectral ordinates with respect to Eurocode 8. The less conservative short-period Eurocode 8 damping scaling is prominent in vertical spectral ordinates and at large damping values. These discussions advocate the reconsideration of damping scaling in the future modifications of Eurocode 8 ground-motion definition.

The last figure (Fig. 4) in this section shows the significance of aleatory variability in DSF estimates. The left and right panels in Fig. 4 depict median and $\pm$ sigma horizontal and vertical DSF estimates of the proposed model for $\beta = 1$ and 10 %. The chosen scenario event has a moment magnitude of M_w 7.0; however, it is noted that our sigma is independent of magnitude. The site resembles stiff soil conditions ($V_{S30} = 400$ m/s) and it is located $R_{JB} = 10$ km from a strike-slip fault. The comparative plots indicate that the aleatory variability is more significant in vertical DSF amplitudes.

4 Vertical-to-horizontal (V/H) spectral amplitude predictive model

The vertical-to-horizontal PSA GMPE presented in this section differs from the recently proposed vertical ground-motion models in Europe.[2] The proposed model is capable of estimating V/H ratios for all site conditions that makes it different from the V/H models of Edwards et al. (2011) and Poggi et al. (2012) that are valid for rock and soft sites, respectively. Although the empirical V/H model proposed in this study as well as the one proposed by Bommer et al. (2011) are based on European datasets, the GMPE of this study is developed on a more comprehensive and recently revised pan-European ground-motion database (Akkar et al. 2013c). The other major difference between the V/H model of this study and Bommer et al. (2011) is the site response function. The site term of our model is a continuous function of V_{S30} and considers soil nonlinearity whereas Bommer et al. (2011) use a set of dummy parameters to account for the site effects. Besides, the proposed V/H model is fully compatible with the pan-European 5 %-damped horizontal PSA GMPE of Akkar et al. (2013a,b) because the database, thus all metadata and record processing, is common in both models. This property makes our model more useful in probabilistic seismic hazard assessment of broader Europe

[2] This paper only discusses the most recent vertical ground-motion models in Europe. The reader is referred to Bommer et al. (2011) for a detailed literature review on the entire progress of pan-European vertical GMPEs.

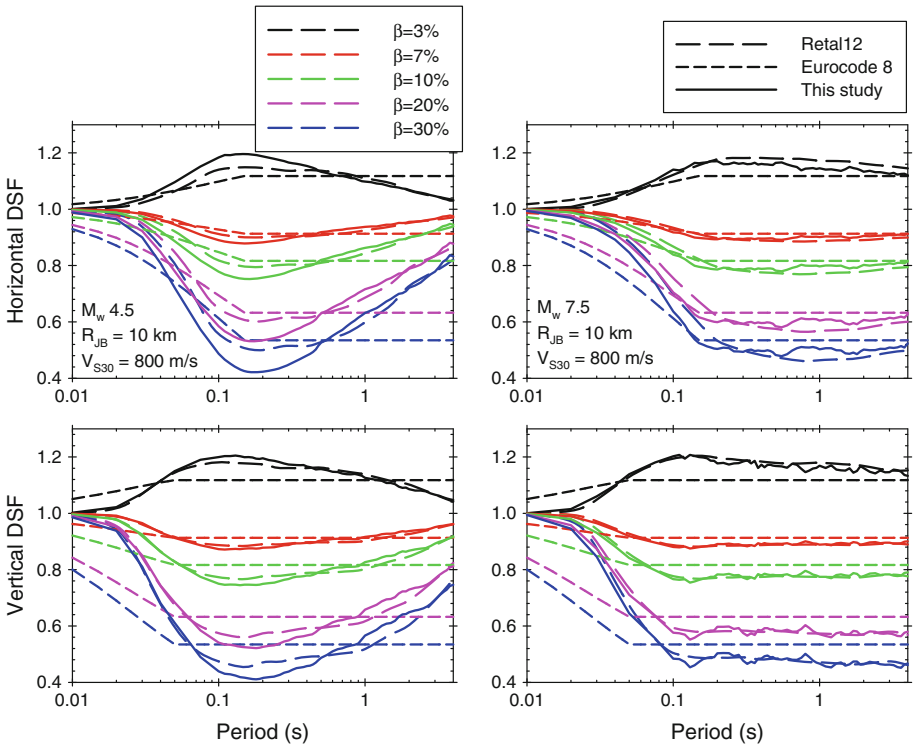

Fig. 3 Horizontal (*top row*) and vertical (*bottom row*) DSF values of the proposed model as well as those of Rezaeian et al (2012; Retal12) and Eurocode 8 (CEN 2004) for M_w 4.5 (*left panel*) and M_w 7.5 (*right panel*) at $R_{JB} = 10$ km for a rock site of $V_{S30} = 800$ m/s

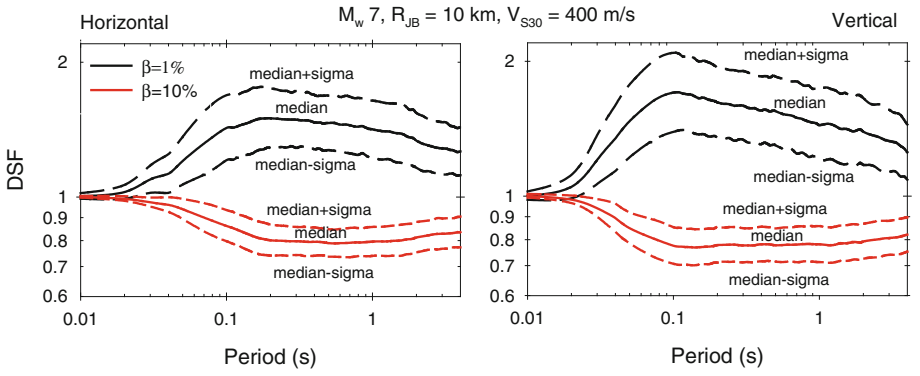

Fig. 4 Effect of aleatory variability on horizontal and vertical DSF models proposed in this study

region for computing consistent horizontal and vertical pseudo-acceleration spectral ordinates for scenario-specific engineering studies. The presented V/H GMPE is also different from the model proposed by Ambraseys et al. (2005) as the latter developed an independent GMPE for the estimation of vertical spectral ordinates. The approach in Ambraseys et al. (2005) may produce vertical and horizontal spectral accelerations that are controlled by different

earthquake scenarios. As discussed briefly in introduction, different controlling earthquake scenarios for horizontal and vertical ground motions may cause practical difficulties in seismic design and performance assessment procedures that utilize compatible horizontal and vertical spectral demands. This shortcoming is prevailed by using V/H models as suggested in this paper. The particular features of the proposed V/H GMPE are described in the following paragraphs.

The proposed V/H model (Eq. 5) uses a functional form similar to that of Akkar et al. (2013a,b) horizontal GMPE for producing compatible vertical PSA as emphasized throughout the text. The magnitude scaling consists of a quadratic magnitude term as well as a hinging magnitude (c_1)—this is different than the coefficient defined in the DSF models—to account for magnitude saturation effects. The model considers magnitude dependency in geometrical spreading and describes the soil effects with a nonlinear site function that is based on V_{S30} and PGA at the reference rock site ($V_{REF} = 750$ m/s). The effect of faulting mechanism on V/H is addressed by dummy variables F_N and F_R that are unity for normal and reverse faults, respectively, and zero otherwise.

$$\ln(V/H) = \begin{cases} a_1 + a_2(M_w - c_1) + a_3(8.5 - M_w)^2 + [a_4 + a_5(M_W - c_1)] \\ \quad \ln\left(\sqrt{R_{JB}^2 + a_6^2}\right) + a_8 F_N + a_9 F_R + \ln(S) \qquad \text{for } M_w \le c_1 \\ a_1 + a_7(M_w - c_1) + a_3(8.5 - M_w)^2 + [a_4 + a_5(M_W - c_1)] \\ \quad \ln\left(\sqrt{R_{JB}^2 + a_6^2}\right) + a_8 F_N + a_9 F_R + \ln(S) \qquad \text{for } M_w > c_1 \end{cases} \tag{5a}$$

$$\ln(S) = \begin{cases} a_{10} \ln\left(\dfrac{V_{S30}}{V_{REF}}\right) - a_{11} \\ \quad \ln\left[\dfrac{PGA_{REF} + c\left(\dfrac{V_{S30}}{V_{REF}}\right)^n}{(PGA_{REF} + c)\left(\dfrac{V_{S30}}{V_{REF}}\right)^n}\right] \qquad \text{for } V_{S30} \le V_{REF} \\ a_{10} \ln\left[\dfrac{\min(V_{S30}, 1000)}{V_{REF}}\right] \qquad \text{for } V_{S30} > V_{REF} \end{cases} \tag{5b}$$

$$\ln(PGA_{REF}) = \begin{cases} \text{for } M_w \le c_1 \quad 1.85329 + 0.0029(M_w - c_1) - 0.02807(8.5 - M_w)^2 \\ \quad +[-1.23452 + 0.2529(M_W - c_1)]\ln\left(\sqrt{R_{JB}^2 + 7.5^2}\right) - 0.1091 F_N + 0.0937 F_R \\ \text{for } M_w > c_1 \quad 1.85329 - 0.5096(M_w - c_1) - 0.02807(8.5 - M_w)^2 \\ \quad +[-1.23452 + 0.2529(M_W - c_1)]\ln\left(\sqrt{R_{JB}^2 + 7.5^2}\right) - 0.1091 F_N + 0.0937 F_R \end{cases} \tag{5c}$$

The regression coefficients a_1 to a_{10} are computed from mixed-effects regression algorithm of Abrahamson and Youngs (1992). The magnitude and source-to-site distance measures are moment magnitude (M_w) and Joyner–Boore distance (R_{JB}) that are now almost standard in most of the predictive models in Europe. The hinging magnitude c_1 is taken as 6.75 as in the case of Akkar et al. (2013a,b) horizontal GMPE after making several observations on the empirical data trend. The fictitious depth and the coefficients of linear magnitude terms (a_2 and a_7) are held fixed for the entire period range for a smooth spectral shape. The site amplification function, designated by ln(S) in Eq. 5b, includes both linear and nonlinear soil amplification. The nonlinearity is considered by the reference horizontal peak ground acceleration (PGA_{REF}) that is computed for $V_{S30} = 750$ m/s (see Eq. 5c). The unit of PGA_{REF} is in terms of gravitational acceleration, g. The V_{S30} value of 750 m/s defines reference rock conditions in the V/H nonlinear site model, which is also the case in the nonlinear site

function of Akkar et al. (2013a,b) horizontal GMPE. The regression coefficients c, n, and a_{11} are adopted from the Sandıkkaya et al. (2013) site model.

5 Evaluation of proposed V/H GMPE with emphasis on nonlinear soil behavior

The nonlinear site behavior in the V/H model deserves some more discussion. The soil amplification of V/H inherently depends on the site behavior of vertical and horizontal acceleration components and it has yet to be better understood. In horizontal ground motions, the site-dependent amplification is represented by linear and nonlinear site terms. The latter term dominates at high ground-motion intensity levels and when V_{S30} attains low values (Choi and Stewart 2005; Walling et al. 2008; Sandıkkaya et al. 2013). On the other hand, there is no clear evidence on the nonlinear site behavior of vertical ground motions. To our knowledge, the significance of nonlinearity in vertical ground motions has never been studied in detail from a GMPE perspective. Almost all independent vertical ground-motion GMPEs (e.g., Campbell and Bozorgnia 2003; Ambraseys et al. 2005; Cauzzi and Faccioli 2008) consider linear site behavior. Of the recently developed V/H GMPEs, Gülerce and Abrahamson (2011) account for nonlinear soil behavior whereas Bommer et al. (2011) disregard nonlinear site effects in V/H estimates.

From a theoretical view point, modeling nonlinear site effect for horizontal and vertical ground motions is always possible provided that the strong-motion metadata contains sufficient and reliable information on the modeling parameters. Observations on the empirical data trend as well as the significance of nonlinear term after regressions would define their potential impact in vertical and horizontal ground-motion estimates. The common assumption of log-normal distribution in horizontal and vertical ground motions imposes the same probability distribution for their ratio, which constitutes the basis of our logarithmic V/H model as given in Eq. (5a). Since site effects of horizontal and vertical ground motions are additive in the logarithmic V/H model, the contributions of linear and nonlinear site terms would control the overall V/H behavior and this should be mapped on to the estimated vertical ground motions.

The above discussion is visually illustrated by Figs. 5 and 6 that show the median estimates of vertical PGA and PSA at T = 0.05, 0.1 and 0.2 s. The vertical ground motions significantly affect the amplitudes of these high-frequency spectral ordinates as discussed in the previously cited references. The figures compare the median vertical ground-motion estimates of three alternative predictive models. The first predictive model is the one proposed in this study (designated as "Nonlinear V/H" on the figures). The second model constrains a_{11} to zero to disregard nonlinear site effects in Eq. (5b) and it is called as "Linear V/H" in Figs. 5 and 6. The last GMPE directly estimates the vertical spectral ordinates and it is defined as "Independent Vertical" on the plots. All three models are derived from the database used in this study. The third GMPE (independent vertical) disregards nonlinear site effects as neither the regression analysis nor the empirical data trends supported the effects of nonlinear soil behavior on vertical ground motions. Figure 5 shows the distance-dependent variation of median vertical ground-motion estimates from these alternative GMPEs for a generic rock site (V_{S30} = 750 m/s) for M_w 7.5 and M_w 5.5. The style-of-faulting is chosen as strike-slip for the scenario earthquakes. Figure 6 displays the same plots for a soft site represented by V_{S30} = 250 m/s. The median horizontal spectral ordinates of the Akkar et al. (2013a,b) GMPE are modified by the linear and nonlinear V/H models to obtain the corresponding median vertical ground-motion estimates.

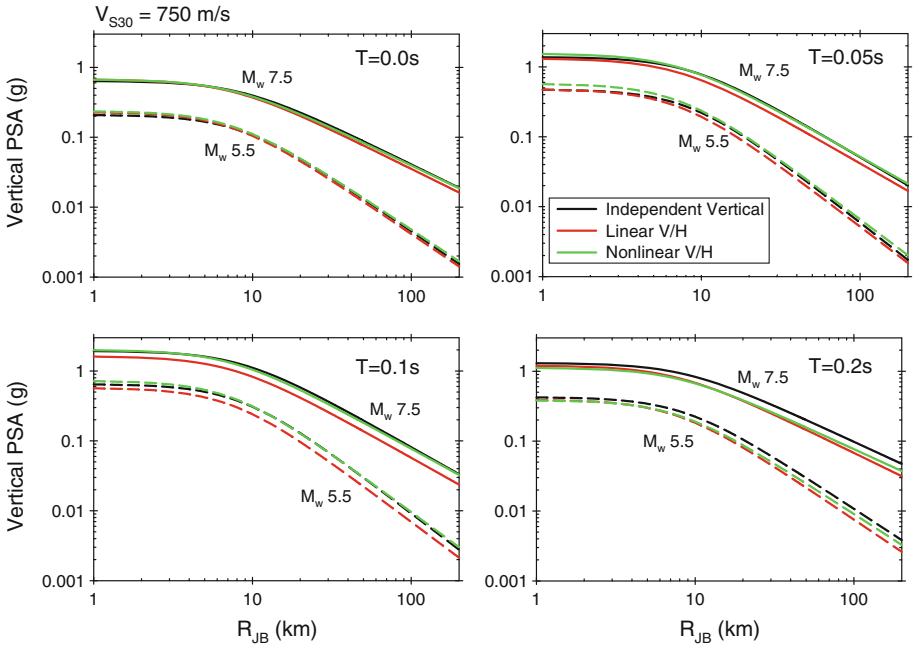

Fig. 5 Median V/H estimates computed from linear and nonlinear V/H models as well as an independent vertical ground-motion GMPE. The chosen site represents generic rock conditions ($V_{S30} = 750$ m/s). The comparisons are done for M_w 7.5 (*solid lines*) and M_w 5.5 (*dashed lines*) earthquakes generated by a strike-slip fault

The comparative plots in Fig. 5 indicate that all three GMPEs yield very similar vertical ground motions regardless of the variations in magnitude. The vertical ground-motion estimates from linear V/H model are slightly smaller with respect to the predictions of the other two GMPEs in many cases. The plots in Fig. 6 depict very similar vertical ground-motion estimates for nonlinear V/H and independent vertical GMPEs. The median plots almost overlap with each other for these models. The observed differences in linear V/H become more visible in Fig. 6. The observations from Figs. 5 and 6 suggest that the nonlinear site effects are not prominent in vertical ground motions regardless of the variations in magnitude and distance. Thus, independent vertical GMPEs may overlook nonlinear soil behavior. However, consideration of soil nonlinearity in V/H models provides a control over the nonlinear soil effects of horizontal ground motions. This approach results in mimicking the genuine variations in the vertical ground-motion demands when V/H ratios are implemented together with the horizontal GMPEs. Under the light of these discussions and because we prefer providing a V/H model instead of an independent vertical GMPE for consistency between horizontal and vertical earthquake scenarios, the site amplification function given in Eq. (5b) considers the nonlinear soil behavior.

The proposed model is also evaluated in terms of classical residual analysis. Figure 7 shows the within-event and between-event residuals for $T = 0.2$ s. The within-event residuals (left panel) are plotted in terms of V_{S30} whereas between-event residuals (right panel) are plotted for moment magnitude, M_w. The plots also show the average residuals for a set of predetermined V_{S30} and M_w intervals. The V_{S30} intervals have a uniform spacing of 180 m/s for $V_{S30} \leq 900$ m/s. A single average of between-event residuals is computed for $V_{S30} > 900$

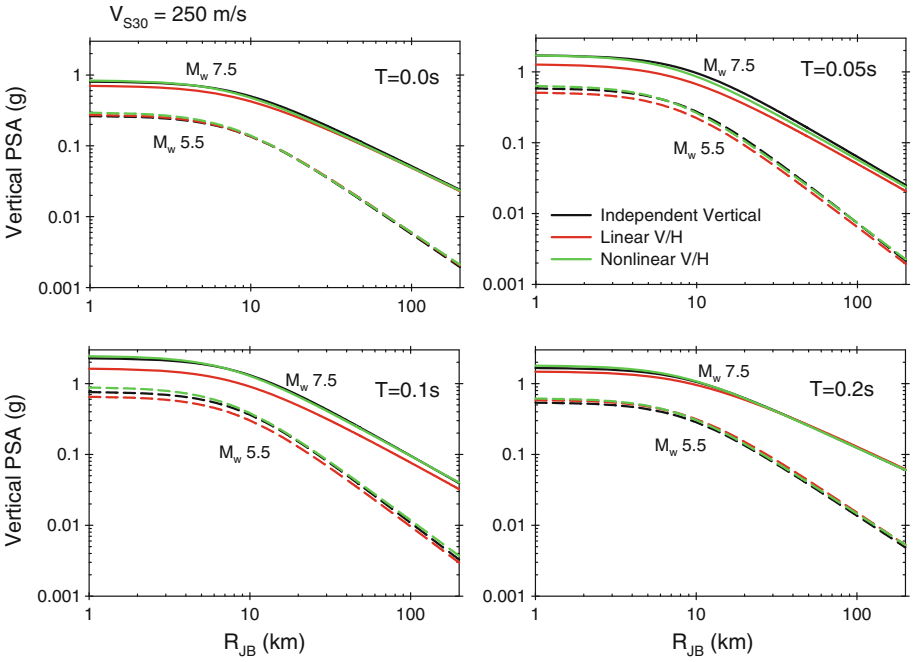

Fig. 6 Median V/H estimates computed from linear and nonlinear V/H models as well as an independent vertical ground-motion GMPE. The chosen site represents generic rock conditions (V_{S30} = 250 m/s). The comparisons are done for M_w 7.5 (*solid lines*) and M_w 5.5 (*dashed lines*) earthquakes generated by a strike-slip fault

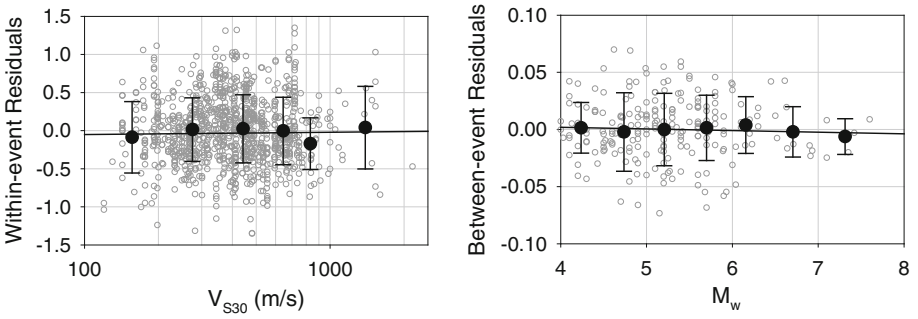

Fig. 7 Between- and within-event residual distributions for the V/H GMPE at T = 0.2s. The between-event residuals are plotted in terms of M_w whereas within-event residuals are given as a function of V_{S30}

m/s as the data are sparse after this V_{S30} value. The M_w intervals are incremented by 0.5 units between $4 \leq M_w \leq 7$. The between-event residuals are also represented by a single average after M_w 7.0 due to sparse data distribution. The residuals are randomly distributed over the magnitude and V_{S30} range considered in this study. Their averages for the pre-determined intervals fluctuate about zero. These observations suggest unbiased estimates of the proposed V/H GMPE. The random distribution of within-event residuals can be interpreted as the satisfactory performance of the preferred nonlinear site model. We produced similar residual plots for other spectral periods and the trends discussed for T = 0.2 s are also valid for these figures. We did not show them in the paper for space considerations.

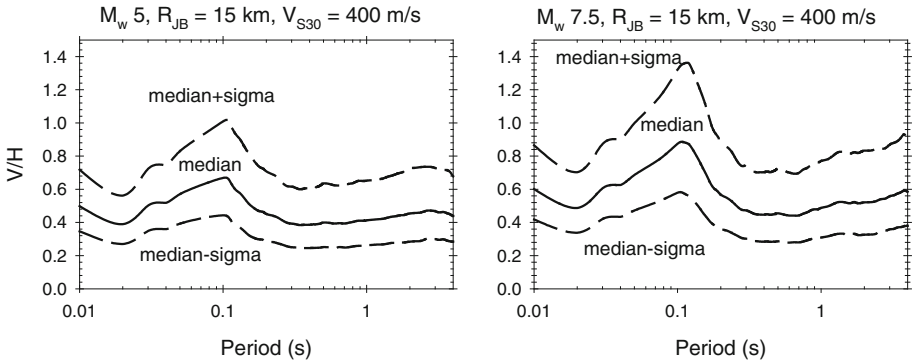

Fig. 8 Effect of aleatory variability in the proposed V/H GMPE

Figure 8 shows the influence of aleatory variability on V/H estimates of the proposed model. The plots in Fig. 8 are prepared for earthquake scenarios of M_w 5 (left panel) and M_w 7.5 (right panel). The chosen V_{S30} value assumes stiff site conditions ($V_{S30} = 400$ m/s). The fictitious site is at a distance of $R_{JB} = 15$ km from strike-slip fault. The median $\pm$ sigma curves indicate that the variations in vertical ground-motion amplitudes can be significant due to aleatory variability. This variation should be considered seriously in vector-valued probabilistic hazard studies. Table 5 lists the regression coefficients of the V/H GMPE for the same periods as of horizontal and vertical DSF models. The full list of regression coefficients for the entire spectral periods are given in the electronic supplementary to this article.

6 Details of the proposed V/H GMPE and its comparisons with the previous pan-European model

The proposed V/H model is studied further to have better insight about its behavior. Figure 9 shows the median V/H estimates for T = 0.1s under the variation of fundamental estimator parameters (i.e., M_w, R_{JB} and V_{S30}). However, the discussions made here generally hold for the entire period range considered in this study. Figure 9a displays the magnitude-dependent V/H variation for different R_{JB} values. The assumed site condition is rock ($V_{S30} = 750$ m/s) and the chosen SoF is strike-slip in this case. The median V/H curves indicate that for magnitudes up to M_w 6 (acts like a node in this panel) one would expect larger V/H values with increasing distance. Thus, horizontal spectral ordinates tend to decay faster with respect to vertical spectral ordinates for small to moderate size events. This trend changes for $M_w >$ 6 and increase in distance yields a decrease in V/H ratios that eventually indicates slower decay of horizontal spectral ordinates with respect to their vertical counterparts. Fig. 9b that shows the distance-dependent behavior of V/H for a set of magnitude values supports the observations in Fig. 9a. The increase in distance yields larger V/H for magnitudes up to M_w 6 that is reversed for $M_w > 6$. As pointed out in Fig. 9a, the horizontal spectral ordinates of small to moderate size events ($M_w < 6$) attenuate faster with respect to their vertical counterparts and this trend reverses as magnitude becomes larger. The median V/H curve for M_w 6 is almost insensitive to variations in distance, which explains its "nodal" position in Fig. 9a. Figure 9c that shows the particular influence of V_{S30} on V/H suggests that the vertical spectrum tends to attain larger values for soft to very soft sites ($V_{S30} < 350$ m/s) and large magnitudes ($M_w > 7$). As the site gets stiffer the variations in V/H are mild and stable.

Table 5 Period-dependent regression coefficients of the V/H ground-motion model for the selected periods. Period-independent coefficients are given in the footnote*

Period (s)	a_1	a_3	a_4	a_8	a_9	a_{10}	a_{11}	ϕ^{**}	τ^{**}	σ^{**}
PGA	−0.55429	0.03124	−0.01172	0.04174	0.00483	0.2153	−0.28846	0.3578	0.0663	0.3639
PGV	−0.83717	0.0253	0.06389	0.10829	0.10998	0.36054	−0.19688	0.3655	0.0204	0.3661
0.01	−0.54467	0.03109	−0.01347	0.04465	0.00688	0.20949	−0.28685	0.3571	0.0747	0.3648
0.02	−0.46655	0.03099	−0.02821	0.04626	0.00711	0.21464	−0.28241	0.3558	0.0844	0.3657
0.03	−0.25416	0.03095	−0.07133	0.04137	−0.00933	0.20684	−0.26842	0.3613	0.0969	0.3741
0.04	−0.03087	0.02804	−0.10768	0.02432	−0.06283	0.17531	−0.24759	0.373	0.1161	0.3907
0.05	0.09261	0.02211	−0.12033	−0.01097	−0.0786	0.11306	−0.22385	0.3922	0.1259	0.4119
0.075	−0.02755	0.01822	−0.07373	0.00883	−0.09063	0.06983	−0.17525	0.405	0.1377	0.4278
0.1	−0.2157	0.01558	−0.02512	0.01238	−0.15905	0.0824	−0.29293	0.4103	0.1701	0.4442
0.15	−0.79732	0.02578	0.06757	0.03577	−0.04592	0.15636	−0.39551	0.4455	0.1057	0.4579
0.2	−1.02981	0.03463	0.08653	0.05953	−0.00392	0.21837	−0.44644	0.4404	0.0816	0.4479
0.3	−1.14208	0.0382	0.09311	0.10302	0.05769	0.31643	−0.4573	0.4454	0.0249	0.4461
0.4	−1.09718	0.03975	0.09001	0.04878	0.07534	0.38181	−0.43008	0.4468	0.0828	0.4544
0.5	−1.0642	0.0401	0.08691	0.06349	0.09199	0.40009	−0.37408	0.4557	0.0674	0.4607
0.75	−0.89263	0.0349	0.0751	0.07806	0.10535	0.44592	−0.28957	0.4584	0.0256	0.4591
1	−0.73533	0.03063	0.0609	0.08829	0.11555	0.50958	−0.28702	0.4508	0.0252	0.4515
1.5	−0.70636	0.03203	0.0467	0.06958	0.12575	0.4262	−0.24695	0.4462	0.0864	0.4545
2	−0.62766	0.03247	0.0332	0.06344	0.13595	0.42834	−0.17336	0.4632	0.0518	0.4661
3	−0.42904	0.02433	0.0197	0.0934	0.14271	0.51101	−0.13336	0.4337	0.0686	0.4391
4	−0.35034	0.01392	0.00738	0.19948	0.15823	0.54615	−0.07749	0.4427	0.0821	0.4502

*$a_2 = 0.33$; $a_5 = -0.04$; $a_6 = 5$; $a_7 = 0.19$; $c_1 = 6.75$; $V_{REF} = 750\,\text{m/s}$, $c = 2.5$; $n = 3.2$

** ϕ, τ and σ refer to within-event, between-event and total standard deviations, respectively

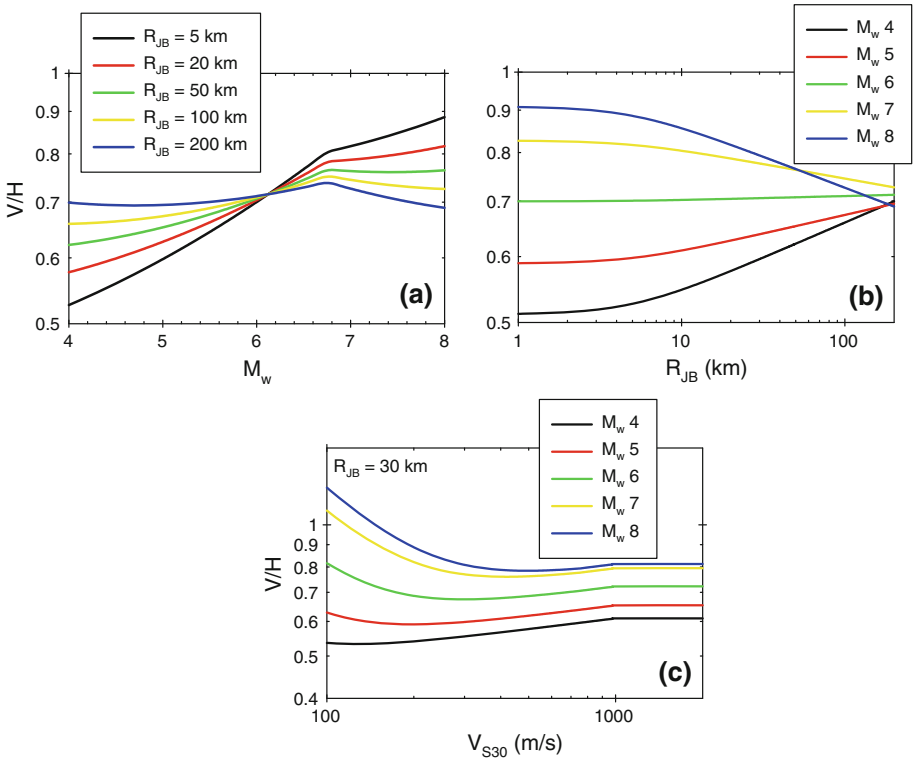

Fig. 9 Median V/H variations of the proposed model in terms major estimator parameters for T = 0.1s

The proposed model is also compared with the recent pan-European V/H GMPE that is developed by (Bommer et al. 2011; BAK11). The magnitude scaling is linear and geometrical spreading does not consider a magnitude dependent slope in BAK11. It disregards the soil nonlinearity in V/H estimates. Figure 10 compares the median V/H estimates of these two models. The comparisons are made for median V/H trends as this spectral quantity is used while constructing the horizontal spectrum compatible vertical spectral ordinates for scenario-specific PSHA. The details of this procedure are described in the subsequent sections. The spectral comparisons in Fig. 10 are done for $R_{JB} = 10$ km for M_w 5 and M_w 7.5 (left and right columns, respectively). A strike-slip fault is used in the scenario earthquakes as in the case of previous examples. The top row panels compare the median V/H estimates for $V_{S30} = 800$ m/s (generic rock site) whereas the bottom row comparisons are plotted for $V_{S30} = 255$ m/s (soft soil). The median V/H estimates of the proposed model depict differences with respect to BAK11. However, the differences are not substantial. Our model tends to estimate larger V/H ratios towards longer periods for larger magnitudes. The opposite holds for small magnitudes and BAK11 yields larger V/H estimates particularly for softer sites. The discrepancies between the median V/H estimates of BAK11 and the proposed model can be the attributes of different functional forms as well as the size and resolution of databases although they are originated from the same region. This study uses a more complicated functional form that considers magnitude-dependent geometrical spreading as well as linear and nonlinear soil behavior as a function of continuous V_{S30}. These features are not included in BAK11 due to insufficient meta-

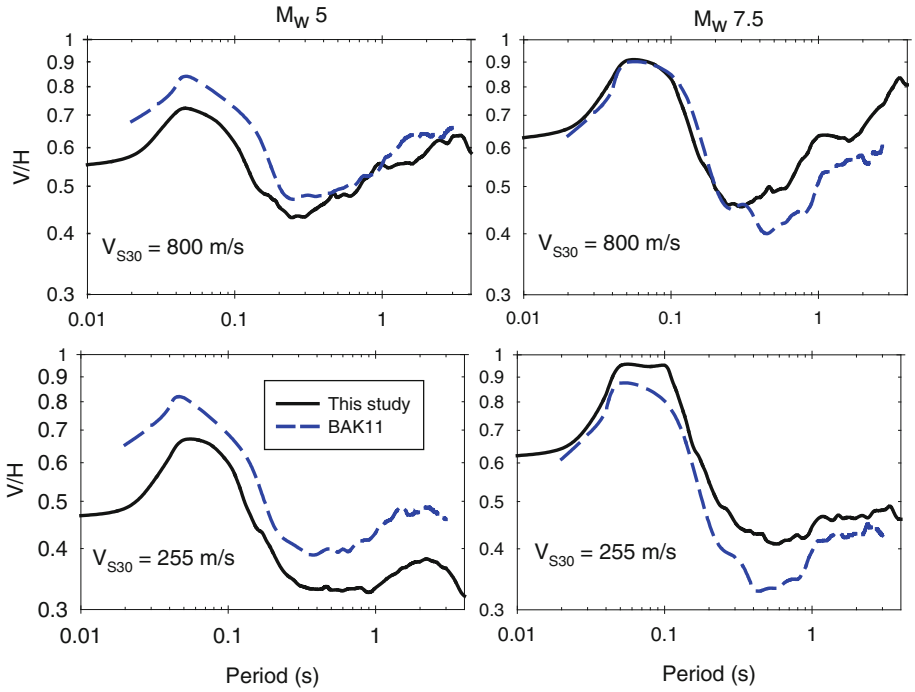

Fig. 10 Comparison of the proposed equation with Bommer et al. (2011; BAK11) V/H model for different magnitudes and site conditions at $R_{JB} = 10$ km

data features in their database. Although BAK11 and this study use strong-motion data collected from broader Europe, the pan-European database used in this study is recently updated and expanded in terms of waveform quality and metadata information (Akkar et al. 2013c).

7 Use of proposed DSF and V/H models for different point-source distance metrics

The proposed DSF and V/H GMPEs use R_{JB} as the source-to-site distance metric. This section provides information on the applicability of these models for point source distance measures (epicentral distance -R_{epi}- and hypocentral distance -R_{hyp}-) as Akkar et al. (2013a,b) GMPEs are developed for estimating horizontal ground motions in R_{epi}, R_{hyp} and R_{JB}. Figure 11 shows median horizontal DSF estimates computed for R_{JB}, R_{epi} and R_{hyp} for a stiff site of $V_{S30} = 400$ m/s. The availability all three distance measures in our strong-motion database enabled us to develop DSF predictive GMPEs for the latter two distance measures. The same functional form as of R_{JB}-based DSF predictive model was used in these GMPEs and same steps were followed in the regressions. The distance range considered in comparisons is up to 200 km. Each raw in Fig. 11 compares the median horizontal DSF estimates of R_{JB}, R_{epi} and R_{hyp} for a specific period. The selected spectral periods for comparisons are T = 0.1 s, T = 0.5 s, T = 1.0 s, T = 2.0 s and T = 4.0 s. They represent the overall spectral period interval of concern in the paper. Each column in Fig. 11 shows a specific magnitude taking values between M_w 4 and M_w 8 with unit increments. The comparisons are shown for 2 and

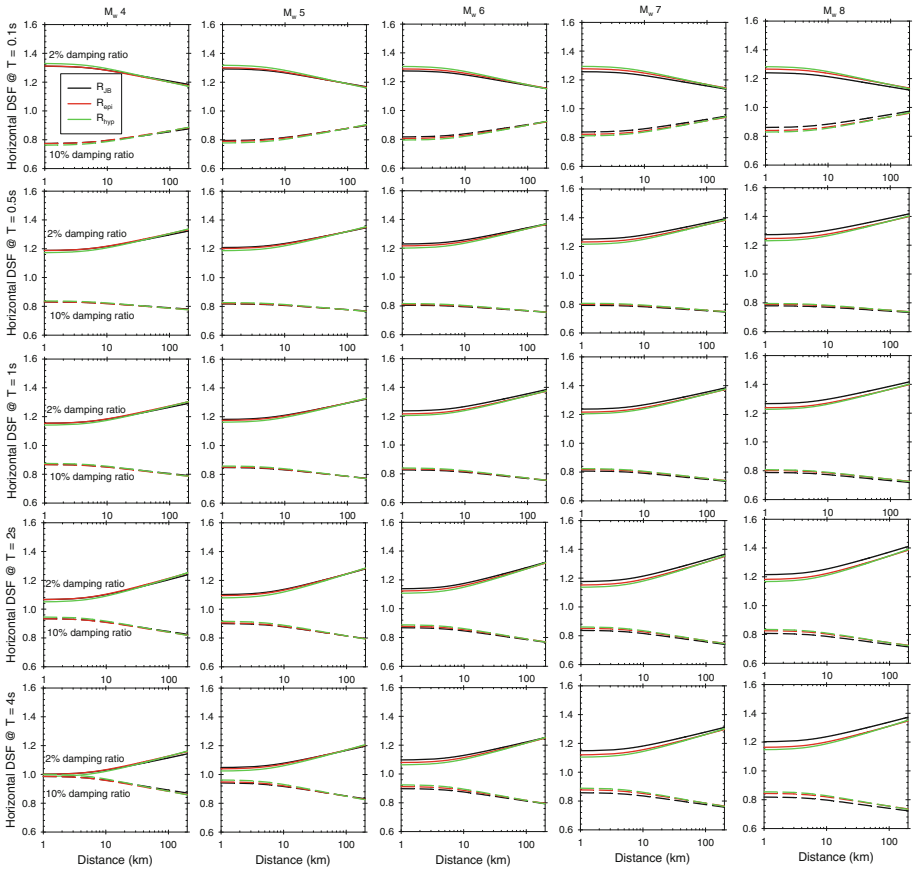

Fig. 11 Comparisons of median horizontal DSF estimates from R_{JB}-, R_{epi}- and R_{hyp}-based GMPEs that are derived from the same strong-motion database. The functional forms of all three GMPEs are the same. The *solid* and *dashed lines* show the comparisons for 2 and 10 % damping, respectively

10 % damping ratios in order not to crowd the panels. The other damping ratios yield similar results to those given in Fig. 11. Figure 12 makes the same comparisons for vertical DSF estimates. The display format in this figure is the same as in Fig. 11. The comparative plots indicate that median horizontal and vertical DSF estimates are practically independent of distance definition. For lightly damped systems (represented by 2 % critical damping in Figs. 11 and 12) and towards large magnitudes, the variations in R_{JB}-based DSF model are slightly different than the median DSF trends of the point-source distance metrics. However, the observed discrepancies are not more than 5 % for the entire distance range. The observations highlighted by these plots are valid for the whole magnitude, period and damping ratios covered in this study. Thus, the overall discussions from Figs. 11 and 12 suggest the general applicability of R_{JB}-based horizontal and vertical DSF GMPEs for the modification of 5 %-damped spectral ordinates of Akkar et al. (2013a,b) without making any adjustments for R_{epi} and R_{hyp}.

Similar comparisons are repeated for the median V/H estimates. Figure 13 shows the median V/H estimates of R_{JB}, R_{epi} and R_{hyp} predictive models. The GMPEs for R_{epi} and R_{hyp} are developed by following the methodology described in the DSF comparisons: same

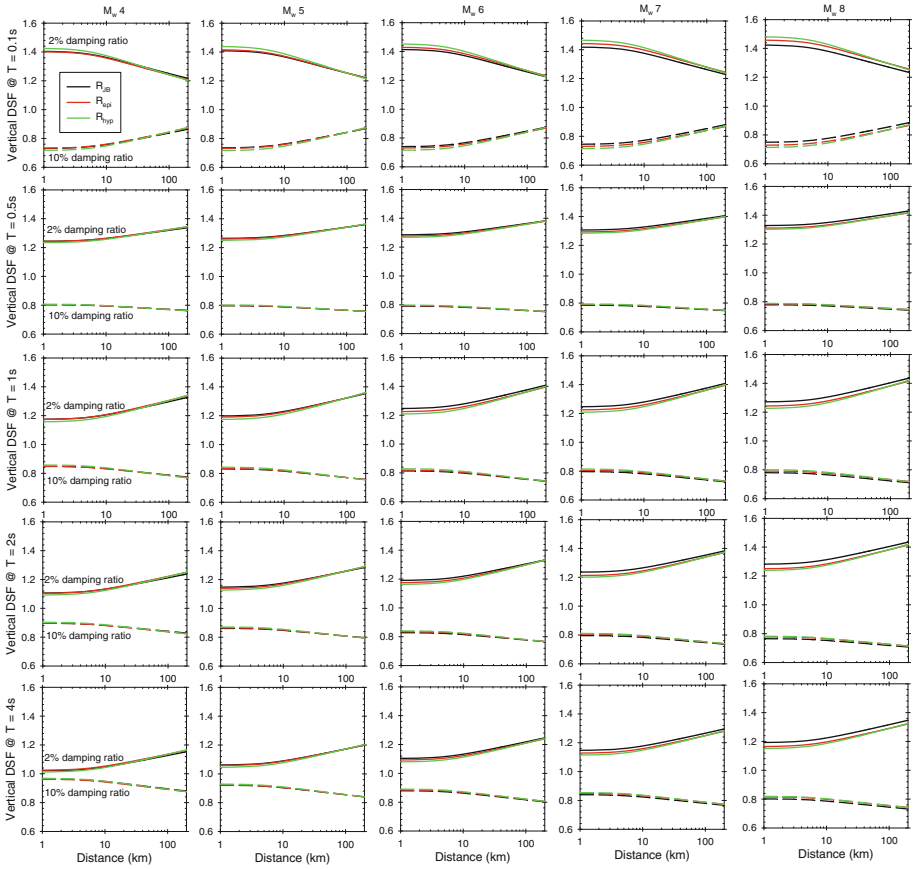

Fig. 12 Comparisons of median vertical DSF estimates from R_{JB}-, R_{epi}- and R_{hyp}-based GMPEs that are derived from the same strong-motion database. The functional forms of all three GMPEs are the same. The *solid* and *dashed lines* show the comparisons for 2 and 10 % damping, respectively

functional forms as of R_{JB}-based GMPE and same type of regression analysis by utilizing the strong-motion database used for developing R_{JB}-based GMPE. The plots in Fig. 13 compare median V/H estimates for the above three distance measures by using the period and magnitude combinations given in Figs. 11 and 12. The comparisons in Fig. 13 display very similar patterns between the median V/H estimates of R_{epi}, R_{hyp} and R_{JB} GMPEs. Although some minor discrepancies in V/H trends do exist between R_{hyp} and the other two distance metrics, we believe that these differences can be neglected for all practical purposes. Thus, one can use our R_{JB}-based V/H model in confidence with the Akkar et al. (2013a,b) horizontal GMPEs of all three distance measures to generate fully consistent vertical ground-motion estimates.

The conclusions derived from the median DSF and V/H comparisons are further investigated by studying the total standard deviations of the DSF and V/H GMPEs that are developed separately for each source-to-site distance metric. The comparative results are shown in Fig. 14. The left and right panels in the first row of Fig. 14 show the period-dependent variation of total sigma for horizontal and vertical DSF GMPEs. The panel in the second row displays same type of comparisons for V/H model. The information inferred from Fig. 14 once again

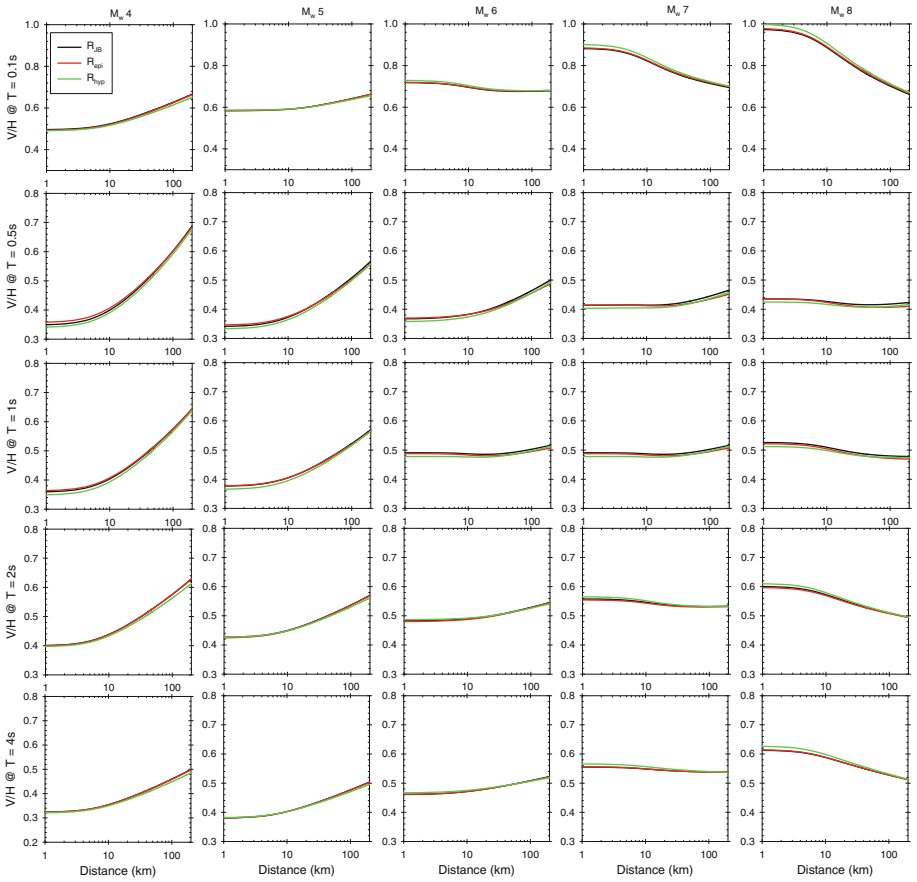

Fig. 13 Comparisons of median V/H estimates from R_{JB}-, R_{epi}- and R_{hyp}-based GMPEs that are developed from the same database. The functional forms of the predictive models are the same

justifies that any existing difference among the three considered distance measures becomes immaterial for DSF and V/H ratio estimates.

8 Developing consistent scenario-based horizontal and vertical pseudo-acceleration spectra

The use of V/H GMPEs together with conditional mean spectrum (CMS; Baker 2011) yields consistent scenario-based horizontal and vertical design spectra (Gülerce and Abrahamson 2011). CMS has the ability of representing more realistic scenario-based horizontal seismic demands as it accounts for the correlation of ground-motion variability at different spectral periods. When V/H model is considered together with CMS, the proper handling of horizontal and vertical ground-motion variability would yield a vertical spectrum that represents consistent vertical seismic demands with the horizontal earthquake scenario. The consistent horizontal and vertical spectra will essentially lead to more realistic selection and scaling of horizontal and vertical ground motions for a specific target earthquake scenario.

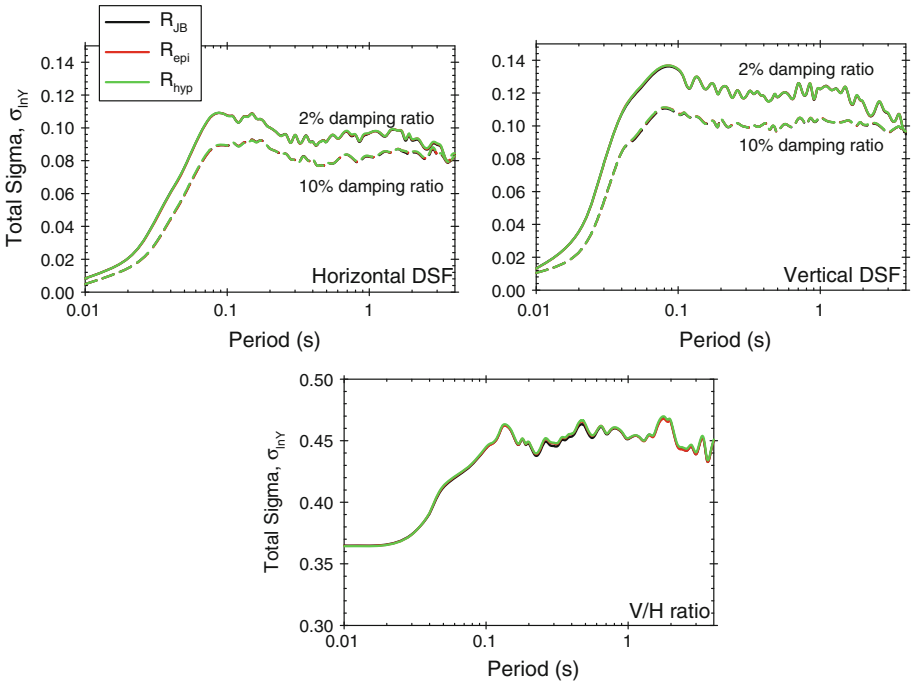

Fig. 14 Comparison of total standard deviations of DSF (*top row*) and V/H (*bottom row*) GMPEs developed for different distance measures

The proposed V/H model is compatible with the Akkar et al. (2013a,b) GMPE derived for horizontal PSA as both studies used exactly the same ground-motion database. Thus, both GMPEs can be employed together for the calculation of consistent CMS for horizontal and vertical ground motions. The complete form of consistent horizontal and vertical CMS is given in Eq. (6) (Baker 2011; Gülerce and Abrahamson 2011).

$$\mathrm{CMS_H}(\mathrm{T_0}, \mathrm{T}) = \mu_{\mathrm{H}}(\mathrm{T}) \cdot \exp\left(\rho_{\mathrm{H}}(\mathrm{T_0}, \mathrm{T})\, \varepsilon(\mathrm{T_0}) \sigma_{\mathrm{H}}(\mathrm{T})\right) \tag{6a}$$

$$\mathrm{CMS_V}(\mathrm{T_0}, \mathrm{T}) = \mathrm{CMS_H}(\mathrm{T_0}, \mathrm{T}) \cdot \mu_{\mathrm{V/H}}(\mathrm{T}) \cdot \exp\left(\rho_{\mathrm{H,V/H}}(\mathrm{T_0}, \mathrm{T}) \cdot \sigma_{\mathrm{V/H}}(\mathrm{T})\right) \tag{6b}$$

In the above expressions $\mu_{\mathrm{H}}(\mathrm{T})$ is the median estimates of the horizontal GMPE for the most contributing earthquake scenario identified after deaggregation analysis for the reference period $\mathrm{T_0}$. The parameter $\sigma_{\mathrm{H}}(\mathrm{T})$ is the total standard deviation of the horizontal GMPE. $\varepsilon(\mathrm{T_0})$ is the number of standard deviations between the target spectral ordinate at $\mathrm{T_0}$ and median ground-motion estimation at the same period for the most contributing earthquake scenario. The correlation coefficient between epsilons at spectral period T and $\mathrm{T_0}$ is defined by $\rho_{\mathrm{H}}(\mathrm{T_0}, \mathrm{T})$. Table 6 gives the correlation coefficient matrix, $\rho_{\mathrm{H}}(\mathrm{T_0}, \mathrm{T})$, for the selected spectral periods using the Akkar et al. (2013a,b) horizontal GMPE. The entire correlation coefficient matrix for the whole set of spectral periods is given in the electronic supplement.

The simplified vertical CMS, $\mathrm{CMS_V}(\mathrm{T_0}, \mathrm{T})$, is computed by multiplying the median V/H, $\mu_{\mathrm{V/H}}(\mathrm{T})$, with the horizontal CMS. Note that $\mu_{\mathrm{V/H}}(\mathrm{T})$ should represent the most contributing horizontal earthquake scenario for internal consistency with the horizontal CMS. These are the first two terms in Eq. (6b). The fully consistent vertical CMS with the horizontal earthquake scenario requires the consideration of ground-motion variability between the horizontal and vertical components that is given as the third multiplicative term in Eq. (6b).

Table 6 Period-dependent correlation coefficient matrix of ρ_H (T_0, T)

Period (s)	PGA	0.01	0.02	0.03	0.04	0.05	0.075	0.1	0.15	0.2	0.3	0.4	0.5	0.75	1	1.5	2	3	4
PGA	1	0.99966	0.99784	0.99198	0.98153	0.96686	0.93427	0.93426	0.91839	0.89789	0.834	0.77764	0.72497	0.62005	0.54546	0.47169	0.46411	0.41179	0.32908
0.01	0.99966	1	0.99846	0.99296	0.98254	0.96805	0.93589	0.93534	0.91889	0.89695	0.83133	0.77413	0.72114	0.61654	0.54163	0.46768	0.46038	0.40905	0.32759
0.02	0.99784	0.99846	1	0.99608	0.98639	0.97227	0.9372	0.93377	0.91548	0.8903	0.82278	0.76584	0.7126	0.61209	0.53828	0.46527	0.45893	0.40769	0.32748
0.03	0.99198	0.99296	0.99608	1	0.99265	0.98009	0.9412	0.9326	0.90798	0.87569	0.7996	0.74114	0.68874	0.59241	0.52024	0.45063	0.44787	0.39706	0.31963
0.04	0.98153	0.98254	0.98639	0.99265	1	0.99187	0.95046	0.93156	0.89437	0.85412	0.76727	0.70701	0.65557	0.56179	0.49043	0.42901	0.43238	0.38185	0.30985
0.05	0.96686	0.96805	0.97227	0.98009	0.99187	1	0.96226	0.93485	0.88309	0.83332	0.73418	0.67099	0.61977	0.52614	0.4561	0.40005	0.40762	0.35783	0.28706
0.075	0.93427	0.93589	0.9372	0.9412	0.95046	0.96226	1	0.96262	0.88845	0.82352	0.70328	0.62602	0.56314	0.45335	0.38092	0.32316	0.3293	0.29077	0.24481
0.1	0.93426	0.93534	0.93377	0.9326	0.93156	0.93485	0.96262	1	0.9362	0.86357	0.72956	0.64721	0.5722	0.45198	0.37881	0.31776	0.32079	0.28606	0.24612
0.15	0.91839	0.91889	0.91548	0.90798	0.89437	0.88309	0.88845	0.9362	1	0.9324	0.78904	0.69128	0.60976	0.47406	0.38947	0.3097	0.30067	0.26877	0.23962
0.2	0.89789	0.89695	0.8903	0.87569	0.85412	0.83332	0.82352	0.86357	0.9324	1	0.88286	0.78939	0.70903	0.56265	0.47235	0.37342	0.35455	0.32109	0.26723
0.3	0.834	0.83133	0.82278	0.7996	0.76727	0.73418	0.70328	0.72956	0.78904	0.88286	1	0.92243	0.8407	0.69909	0.60728	0.48496	0.4531	0.40003	0.30679
0.4	0.77764	0.77413	0.76584	0.74114	0.70701	0.67099	0.62602	0.64721	0.69128	0.78939	0.92243	1	0.93712	0.79936	0.7063	0.57523	0.5291	0.46726	0.35461
0.5	0.72497	0.72114	0.7126	0.68874	0.65557	0.61977	0.56314	0.5722	0.60976	0.70903	0.8407	0.93712	1	0.88239	0.79308	0.66474	0.61543	0.54678	0.42548
0.75	0.62005	0.61654	0.61209	0.59241	0.56179	0.52614	0.45335	0.45198	0.47406	0.56265	0.69909	0.79936	0.88239	1	0.92838	0.80638	0.74174	0.64541	0.53024
1	0.54546	0.54163	0.53828	0.52024	0.49043	0.4561	0.38092	0.37881	0.38947	0.47235	0.60728	0.7063	0.79308	0.92838	1	0.90458	0.84345	0.75232	0.63531
1.5	0.47169	0.46768	0.46527	0.45063	0.42901	0.40005	0.32316	0.31776	0.3097	0.37342	0.48496	0.57523	0.66474	0.80638	0.90458	1	0.9411	0.85455	0.73478
2	0.46411	0.46038	0.45893	0.44787	0.43238	0.40762	0.3293	0.32079	0.30067	0.35455	0.4531	0.5291	0.61543	0.74174	0.84345	0.9411	1	0.91408	0.79894
3	0.41179	0.40905	0.40769	0.39706	0.38185	0.35783	0.29077	0.28606	0.26877	0.32109	0.40003	0.46726	0.54678	0.64541	0.75232	0.85455	0.91408	1	0.93102
4	0.32908	0.32759	0.32748	0.31963	0.30985	0.28706	0.24481	0.24612	0.23962	0.26723	0.30679	0.35461	0.42548	0.53024	0.63531	0.73478	0.79894	0.93102	1

This exponential term consists of the total standard deviation of V/H model and the correlation between the epsilons of horizontal and V/H GMPEs. The total standard deviation is composed of within- and between-event standard deviations. Thus, the correlation between the epsilons of horizontal and V/H GMPEs requires separate consideration of within- and between-event epsilon correlations of horizontal and V/H models. This is given in Eq. (7).

$$\rho_{H,V/H}(T_H, T_{V/H}) = \frac{\phi_H(T_H)\phi_{V/H}(T_{V/H})\rho^{\phi}_{H,V/H}(T_H, T_{V/H}) + \tau_H(T_H)\tau_{V/H}(T_{V/H})\rho^{\tau}_{H,V/H}(T_H, T_{V/H})}{\sigma_H(T_H)\sigma_{V/H}(T_{V/H})} \quad (7)$$

The within-event standard deviations of horizontal and V/H GMPEs are designated as ϕ_H and $\phi_{V/H}$ in Eq. (7), respectively. Similarly, τ_H and $\tau_{V/H}$ stand for the between-event standard deviations of horizontal and V/H GMPEs, respectively. The parameters $\rho^{\phi}_{H,V/H}$ and $\rho^{\tau}_{H,V/H}$ indicate the within- and between-event correlations between the horizontal and V/H GMPEs. Tables 7 and 8 list the within- and between-event correlation coefficient matrices by considering the proposed V/H model and the Akkar et al. (2013a,b) horizontal GMPE. The negative correlations in Tables 7 and 8 indicate an inverse relationship between the expected values of horizontal spectral ordinates and V/H ratios. The full list of within- and between-event correlation coefficient matrices for the whole spectral periods are given in the electronic supplementary to this article.

9 Summary and conclusions

This paper presents ground-motion models to estimate horizontal and vertical damping scaling factors and vertical-to-horizontal PSA ratios by using a subset of the most recent pan-European strong-motion databank that is assembled within the context of SHARE and SIGMA projects (RESORCE; Akkar et al. 2013c). The spectral period range of the GMPEs is between 0.01 and 4.0s. The V/H GMPE additionally estimates horizontal-to-vertical PGA and PGV ratios. The proposed models use the same subset of RESORCE as of Akkar et al. (2013a,b) GMPE that is developed for estimating the 5%-damped horizontal PSA. Thus, the GMPEs presented in this paper complement Akkar et al. (2013a,b) predictive model for its modification for consistent vertical design spectrum as well as horizontal and vertical spectral ordinates of damping ratios other than 5%. Although they are derived for R_{JB}, our verifications showed that these models are equally applicable to Akkar et al. (2013a,b) horizontal ground-motion estimates that are based on R_{epi} and R_{hyp}. The presented models as well as the Akkar et al. (2013a,b) horizontal GMPE, when used together, can serve for consistent vector-valued PSHA in the broader Europe region.

The horizontal and vertical damping scaling models use M_w, R_{JB} and V_{S30} as independent parameters and can modify 5 %-damped spectral ordinates for damping levels ranging between 1 and 50 %. They are applicable of moment magnitudes between 4 and 8 and for distances up to 200 km. These models can also serve for the future updates of damping scaling factors in Eurocode 8 (CEN 2004) as the comparisons given in the paper indicate biased spectrum estimates of Eurocode 8 for very short periods and high damping ratios.

The proposed V/H GMPE considers M_w, R_{JB}, SoF and V_{S30}-based nonlinear site function. The recommended magnitude and distance ranges of the predictive model are the same as those of damping scaling GMPEs. The nonlinear site model has an applicability range of 150 m/s $\leq V_{S30} \leq$ 1200 m/s. As the model is compatible with the Akkar et al. (2013a,b)

Table 7 Period-dependent correlation coefficient matrix for $\rho^{\phi}_{H,V/H}$

Period (s)*	PGA	0.01	0.02	0.03	0.04	0.05	0.075	0.1	0.15	0.2	0.3	0.4	0.5	0.75	1	1.5	2	3	4
PGA	−0.4091	−0.4072	−0.3919	−0.3565	−0.3371	−0.375	−0.316	−0.35	−0.3477	−0.3394	−0.2969	−0.3017	−0.2317	−0.2216	−0.1481	−0.1093	−0.1197	−0.1048	−0.1565
0.01	−0.4083	−0.4074	−0.3921	−0.357	−0.338	−0.3754	−0.3172	−0.3502	−0.3484	−0.3395	−0.2958	−0.2995	−0.2301	−0.2222	−0.1479	−0.1081	−0.1192	−0.1046	−0.1565
0.02	−0.4035	−0.4028	−0.3895	−0.354	−0.3365	−0.3749	−0.3181	−0.3487	−0.3485	−0.3395	−0.2943	−0.2933	−0.2255	−0.2228	−0.1489	−0.1104	−0.1222	−0.1077	−0.1585
0.03	−0.3936	−0.3936	−0.3778	−0.3432	−0.3274	−0.3768	−0.3258	−0.356	−0.3485	−0.336	−0.2849	−0.276	−0.2091	−0.207	−0.1392	−0.1066	−0.1204	−0.1065	−0.1559
0.04	−0.3757	−0.3757	−0.3575	−0.3172	−0.3174	−0.3768	−0.3302	−0.3566	−0.3377	−0.3197	−0.2645	−0.2539	−0.1892	−0.1894	−0.1178	−0.1021	−0.1196	−0.1042	−0.1595
0.05	−0.3571	−0.3563	−0.336	−0.2905	−0.2885	−0.3713	−0.3385	−0.3633	−0.339	−0.3215	−0.2576	−0.2403	−0.173	−0.1723	−0.1023	−0.0898	−0.1121	−0.0932	−0.1447
0.075	−0.337	−0.338	−0.318	−0.273	−0.2454	−0.302	−0.3731	−0.3818	−0.3591	−0.3402	−0.2465	−0.2311	−0.1476	−0.1544	−0.0935	−0.057	−0.0767	−0.0621	−0.1177
0.1	−0.3421	−0.3417	−0.3221	−0.286	−0.2591	−0.3023	−0.3095	−0.4159	−0.3978	−0.3512	−0.2378	−0.2327	−0.1466	−0.1416	−0.0764	−0.0418	−0.0591	−0.0416	−0.1013
0.15	−0.3469	−0.344	−0.3306	−0.2963	−0.2655	−0.2952	−0.2542	−0.3283	−0.443	−0.397	−0.2679	−0.2412	−0.1665	−0.168	−0.0969	−0.0357	−0.0307	0.00068	−0.0805
0.2	−0.3593	−0.357	−0.3502	−0.3245	−0.3005	−0.3008	−0.2214	−0.2741	−0.3304	−0.4301	−0.3226	−0.3155	−0.2351	−0.2207	−0.161	−0.0851	−0.0768	−0.048	−0.1101
0.3	−0.3092	−0.3062	−0.307	−0.3097	−0.2846	−0.2438	−0.1493	−0.1705	−0.1756	−0.252	−0.4155	−0.3952	−0.3078	−0.272	−0.1978	−0.1237	−0.1297	−0.1071	−0.1624
0.4	−0.2735	−0.2711	−0.2748	−0.2916	−0.2687	−0.2295	−0.1096	−0.1155	−0.1192	−0.1668	−0.2999	−0.4388	−0.3387	−0.3049	−0.2165	−0.1584	−0.1518	−0.1471	−0.168
0.5	−0.2424	−0.2408	−0.2456	−0.2701	−0.2515	−0.2104	−0.0833	−0.0734	−0.0735	−0.122	−0.2107	−0.3269	−0.3474	−0.3143	−0.2396	−0.1834	−0.1806	−0.1981	−0.2159
0.75	−0.1654	−0.1621	−0.1704	−0.2002	−0.1943	−0.1575	−0.0499	−0.0119	0.01827	−0.0234	−0.1208	−0.1857	−0.1816	−0.3316	−0.2653	−0.2413	−0.2204	−0.2285	−0.2726
1	−0.1261	−0.1227	−0.1334	−0.164	−0.1599	−0.1209	−0.019	−0.0068	0.05126	0.01853	−0.0806	−0.1171	−0.0947	−0.2038	−0.2754	−0.2587	−0.2459	−0.2509	−0.296
1.5	−0.0567	−0.0523	−0.0613	−0.0854	−0.0935	−0.0725	0.02833	0.03924	0.09688	0.0774	−0.0406	−0.0756	−0.0348	−0.0653	−0.0928	−0.2818	−0.2705	−0.2933	−0.3369
2	−0.0545	−0.046	−0.051	−0.0714	−0.0838	−0.0696	0.02018	0.02176	0.08436	0.07474	−0.0513	−0.0764	−0.0421	−0.0465	−0.0397	−0.1758	−0.2967	−0.3127	−0.3511
3	−0.0222	−0.019	−0.0202	−0.0413	−0.0532	−0.0374	0.05473	0.03042	0.08832	0.06402	−0.039	−0.0819	−0.0569	−0.0269	−0.0113	−0.0823	−0.1463	−0.378	−0.4341
4	−0.008	−0.0067	−0.0109	−0.0292	−0.0419	0.00535	0.0713	0.0468	0.08125	0.03232	−0.0738	−0.0826	−0.0546	−0.0172	−0.0313	−0.0691	−0.1195	−0.336	−0.4955

* Periods in the first column are for the horizontal GMPE whereas the periods in the first row belong to the V/H model

Table 8 Period-dependent correlation coefficient matrix for $\rho^{\tau}_{H,V/H}$

Period (s)*	PGA	0.01	0.02	0.03	0.04	0.05	0.075	0.1	0.15	0.2	0.3	0.4	0.5	0.75	1	1.5	2	3	4
PGA	−0.3738	−0.3634	−0.3513	−0.3224	−0.2497	−0.2078	−0.2567	−0.3224	−0.3145	−0.3221	−0.2549	−0.2151	−0.1752	−0.1989	−0.1862	−0.0807	−0.0324	−0.0195	−0.0456
0.01	−0.3732	−0.3638	−0.352	−0.3231	−0.25	−0.2083	−0.2562	−0.3234	−0.3153	−0.3217	−0.2543	−0.215	−0.1751	−0.2004	−0.1874	−0.0799	−0.0333	−0.019	−0.0462
0.02	−0.3726	−0.3627	−0.3523	−0.3226	−0.2545	−0.2184	−0.2661	−0.3325	−0.3181	−0.3183	−0.245	−0.2023	−0.1612	−0.19	−0.1792	−0.0796	−0.0313	−0.0203	−0.0393
0.03	−0.3645	−0.3536	−0.3427	−0.3119	−0.2505	−0.2267	−0.273	−0.3462	−0.324	−0.3233	−0.2428	−0.1877	−0.1473	−0.1826	−0.1711	−0.0838	−0.0349	−0.0215	−0.0312
0.04	−0.3493	−0.339	−0.3265	−0.289	−0.2361	−0.23	−0.2844	−0.3576	−0.3297	−0.3237	−0.2254	−0.165	−0.1296	−0.1753	−0.1584	−0.0967	−0.0505	−0.0276	−0.0202
0.05	−0.3255	−0.3153	−0.3041	−0.2634	−0.2114	−0.218	−0.2797	−0.359	−0.3381	−0.3343	−0.225	−0.1471	−0.1182	−0.1804	−0.1452	−0.0928	−0.0497	−0.0286	−0.0187
0.075	−0.3035	−0.2991	−0.2878	−0.2525	−0.1781	−0.1519	−0.2811	−0.371	−0.3455	−0.3482	−0.2359	−0.1456	−0.1176	−0.1813	−0.1415	−0.0648	−0.0349	−0.0016	−0.0164
0.1	−0.3379	−0.332	−0.3243	−0.2923	−0.2101	−0.1686	−0.2594	−0.3918	−0.374	−0.3576	−0.2455	−0.1575	−0.124	−0.1734	−0.1416	−0.044	−0.0242	0.02349	−0.0347
0.15	−0.3338	−0.323	−0.3183	−0.2885	−0.2086	−0.1652	−0.2029	−0.3046	−0.3959	−0.3697	−0.2437	−0.1893	−0.1213	−0.1583	−0.1609	−0.0456	−0.0237	0.03357	−0.0224
0.2	−0.3325	−0.3239	−0.3153	−0.296	−0.2068	−0.1326	−0.1583	−0.2262	−0.3153	−0.3778	−0.2872	−0.275	−0.1934	−0.1913	−0.2256	−0.0894	−0.0497	−0.0093	−0.0511
0.3	−0.2837	−0.2748	−0.2672	−0.261	−0.169	−0.0544	−0.0836	−0.0925	−0.1458	−0.1832	−0.3141	−0.3606	−0.2722	−0.2377	−0.2564	−0.115	−0.0809	−0.0538	−0.1106
0.4	−0.2579	−0.251	−0.2456	−0.2298	−0.1478	−0.048	−0.0611	−0.0353	−0.1015	−0.1676	−0.251	−0.3956	−0.2842	−0.2737	−0.2442	−0.1293	−0.0988	−0.0873	−0.1128
0.5	−0.2338	−0.2276	−0.2202	−0.2096	−0.1325	−0.0406	−0.0488	−0.0146	−0.045	−0.1196	−0.1753	−0.3377	−0.2987	−0.2742	−0.2318	−0.1316	−0.121	−0.1311	−0.1269
0.75	−0.2004	−0.1943	−0.1876	−0.1746	−0.113	−0.0435	−0.0454	−0.0028	0.01116	−0.0551	−0.0715	−0.1907	−0.1583	−0.2623	−0.1718	−0.1132	−0.127	−0.1277	−0.1176
1	−0.2026	−0.1965	−0.1871	−0.1821	−0.1282	−0.0492	−0.0555	−0.029	0.027	−0.0297	−0.0208	−0.1259	−0.1051	−0.1578	−0.1491	−0.0999	−0.0898	−0.1428	−0.0907
1.5	−0.1856	−0.1766	−0.1677	−0.1599	−0.1229	−0.0632	−0.0479	−0.0541	0.05525	−0.0075	0.02422	−0.0554	−0.0249	−0.0106	0.02375	−0.0614	−0.0238	−0.1382	−0.053
2	−0.1887	−0.1792	−0.1669	−0.1648	−0.1302	−0.0758	−0.0518	−0.0821	0.046	−0.0023	0.03096	−0.0187	−0.0195	0.03288	0.04779	0.01938	−0.0428	−0.1261	−0.0188
3	−0.1625	−0.1601	−0.1538	−0.1547	−0.1155	−0.0687	−0.0383	−0.0911	0.04182	−0.0298	0.04972	0.02461	0.02969	0.09063	0.07666	0.09121	0.0573	−0.1434	−0.0449
4	−0.0832	−0.086	−0.0924	−0.1004	−0.0845	−0.0414	0.06344	−0.0056	0.04267	0.00134	0.07722	0.02463	0.06808	0.14908	0.14995	0.20841	0.08965	−0.0882	−0.178

* Periods in the first column are for the horizontal GMPE whereas the periods in the first row belong to the V/H model

horizontal GMPE we present epsilon-based correlation coefficients for deriving consistent horizontal and vertical CMS for scenario-based hazard studies in Europe and surrounding regions. The V/H model can also be used for future updates of vertical seismic demands in Eurocode 8 (CEN 2004).

Acknowledgments The work presented in this article has been mainly developed within the SHARE (Seismic Hazard Harmonization in Europe) Project funded under contract 226967 of the EC-Research Framework Programme FP7, and within the SeIsmic Ground Motion Assessment (SIGMA) project. The initial draft of this paper benefitted from the suggestions of Prof. Bommer (Imperial College) and Dr. Douglas (BRGM). Dr. Gülerce and the second author made useful discussions on some specific aspects of V/H GMPEs. TUBITAK provided partial funding to the second author for conducting some part of his PhD studies in Grenoble, France. The reviews by an anonymous reviewer and Dr. J. Douglas increased the technical quality of the paper.

References

Abrahamson NA, Silva WJ (1996) Empirical ground motion models. Report to Brookhaven National Laboratory

Abrahamson NA, Youngs RR (1992) A stable algorithm for regression analyses using the random effects model. Bull Seism Soc Am 82:505–510

Akkar S, Bommer JJ (2006) Influence of long-period filter cut-off on elastic spectral displacements. Earthq Eng Struct Dyn 35:1145–1165

Akkar S, Bommer JJ (2007) Prediction of elastic displacement response spectra at multiple damping levels in Europe and the Middle East. Earthq Eng Struct Dyn 36:1275–1301

Akkar S, Sandıkkaya MA, Bommer JJ (2013a) Empirical ground-motion models for point- and extended-source crustal earthquake scenarios in Europe and the Middle East. Bull Earthq Eng. doi:10.1007/s10518-013-9461-4

Akkar S, Sandıkkaya MA, Bommer JJ (2013b) Erratum to: Empirical ground-motion models for point- and extended-source crustal earthquake scenarios in Europe and the Middle East. Bull Earthq Eng. doi:10.1007/s10518-013-9508-6

Akkar S, Sandıkkaya MA, Şenyurt M, Azari Sisi A, Ay BÖ, Traversa P, Douglas J, Cotton F, Luzi L, Godey S (2013c) Reference database for seismic ground-motion in Europe (RESORCE). Bull Earthq Eng. doi:10.1007/s10518-013-9506-8

Ambraseys NN, Douglas J, Sarma SK, Smit PM (2005) Equations for the estimation of strong ground motions from shallow crustal earthquakes using data from Europe and the Middle East: vertical peak ground acceleration and spectral. Bull Earthq Eng 3:54–73

Applied Technology Council, ATC (2010) Modeling and acceptance criteria for seismic design and analysis of tall buildings. ATC72-1, Redwood City, CA

Ashour SA (1987) Elastic seismic response of buildings with supplemental damping. Dissertation, Ph.D, Department of Civil Engineering, University of Michigan, Ann Arbor, MI

Atkinson GM, Pierre JR (2004) Ground-motion response spectra in eastern North America for different critical damping values. Seismo Res Lett 75:541–545

Baker JW (2011) Conditional mean spectrum: tool for ground motion selection. J Struct Eng 137:322–331

Bazzurro P, Cornell CA (2002) Vector-valued probabilistic seismic hazard analysis (VPSHA). In: Proceedings of the 7th US national conference on earthquake engineering, pp 21–25

Berge-Thierry C, Cotton C, Scotti O, Griot-Pommera D-A, Fukushima Y (2003) New empirical attenuation laws for moderate European earthquakes. J Earthq Eng 7:193–222

Bommer J, Elnashai AS, Chlimintzas GO, Lee D (1998) Review and development of response spectra for displacement-based design. ESEE Research Report No. 98–3, Imperial College London

Bommer J, Mendis R (2005) Scaling of spectral displacement ordinates with damping ratios. Earthq Eng Struct Dyn 34:145–165

Bommer JJ, Akkar S, Kale Ö (2011) A model for vertical-to-horizontal response spectral ratios for Europe and the Middle East. Bull Seismol Soc Am 101:1783–1806

Boore DM, Joyner WB, Fumal TE (1993) Estimation of response spectra and peak accelerations from western North American earthquakes: an interim report, US Geological Survey Open-File Report 93–509. Menlo Park, CA

Bozorgnia Y, Campbell KW (2004) The vertical-to-horizontal spectral ratio and tentative procedures for developing simplified V/H and vertical design spectra. J Earthq Eng 4:539–561

BSSC, Building Seismic Safety Council (2009) 2009 NEHRP recommended seismic provisions for new buildings and other structures: part 1, provisions, Federal Emergency Management Agency (P-750), Washington DC

Cameron WI, Green I (2007) Damping correction factors for horizontal ground-motion response spectra. Bull Seismol Soc Am 97:934–960

Campbell KW, Bozorgnia Y (2003) Updated near-source ground motion (attenuation) relations for the horizontal and vertical components of peak ground acceleration and acceleration response spectra. Bull Seismol Soc Am 93:314–331

Cauzzi C, Faccioli E (2008) Broadband (0.05 to 20 s) prediction of displacement response based on worldwide digital records. J Seismol 12:453–475

Choi Y, Stewart JP (2005) Nonlinear site amplification as function of 30m shear wave velocity. Earthq Spectra 21:1–30

Comité Européen de Normalisation, CEN (2004) Eurocode 8, Design of structures for earthquake resistance—part 1: General rules, seismic actions and rules for buildings. European Standard NF EN 1998-1, Brussels

Edwards B, Poggi V, Fäh D (2011) A predictive equation for the vertical-to-horizontal ratio of ground motion at rock sites based on Shear-Wave velocity profiles from Japan and Switzerland. Bull Seismol Soc Am 101:2998–3019

Elnashai AS, Papazoglu AJ (1997) Procedure and spectra for analysis of RC structures subjected to vertical earthquake loads. J Earthq Eng 1:121–155

Faccioli E, Paolucci R, Rey J (2004) Displacement spectra for long periods. Earthq Spectra 20:347–376

Gülerce Z, Abrahamson NA (2011) Site-specific spectra for vertical ground motion. Earthq Spectra 27:1023–1047

Hatzigeorgiou GD (2010) Damping modification factors for SDOF systems subjected to near-fault, far-fault and artificial earthquakes. Earthq Eng Struct Dyn 39:1239–1258

Idriss IM (1993) Procedures for selecting earthquake ground motions at rock sites. Report NIST GCR 93–625, National Institute of Standards and Technology, Washington, DE

Kunnath SK, Erduran E, Chai YH, Yashinsky M (2008) Effect of near-fault vertical ground motions on seismic response of highway overcrossings. J Bridge Eng ASCE 13:282–290

Lin YY, Chang KC (2003) Study on damping reduction factor for buildings under earthquake ground motions. J Struct Eng 129:206–214

Lin YY, Chang KC (2004) Effects of site classes on damping reduction factors. J Struct Eng 130:1667–1675

Lin YY, Miranda E, Chang KC (2005) Evaluation of damping reduction factors for estimating elastic response of structures with high damping. Earthq Eng Struct Dyn 34:1427–1443

Malhotra PK (2006) Smooth spectra of horizontal and vertical ground motions. Bull Seismol Soc Am 96:506–518

Naeim F, Kircher CA (2001) On the damping adjustment factors for earthquake response spectra. Struct Design Tall Build 10:361–369

Newmark NM, Hall WJ (1982) Earthquake spectra and design. Earthquake Engineering Research Institute, Berkeley, CA

Poggi V, Edwards B, Fäh D (2012) Characterizing the vertical-to-horizontal ratio of ground motion at soft-sediment sites. Bull Seismol Soc Am 102:2741–2756

Priestly MJN (2003) Myths and fallacies in earthquake engineering. The Mallet Milne Lecture, IUSS Press, Istituto Universitario di Studi Superiori di Pavia, Pavia, Italy, Revisited

Ramirez OM, Constantinou MC, Kircher CA, Whittaker AS, Johnson MW, Gomez JD, Chrysostomou CZ (2000) Development and evaluation of simplified procedures for analysis and design of buildings with passive energy dissipation systems. Report No: MCEER-00-0010, Multidisciplinary Center for Earthquake Engineering Research, University of New York, Buffalo, NY

Ramirez OM, Constantinou MC, Whittaker AS, Kircher CA, Chrysostomou CZ (2002) Elastic and inelastic seismic response of buildings with damping systems. Earthq Spectra 18:531–547

Rezaeian S, Bozorgnia Y, Idriss IM, Campbell K, Abrahamson N, Silva W (2012) Spectral damping scaling factors for shallow crustal earthquakes in active tectonic regions. PEER 2012/01, Pacific Earthquake Engineering Research Center, University of California, Berkeley, CA

Sandıkkaya MA, Akkar S, Bard P-Y (2013) A nonlinear site amplification model for the new pan-European ground-motion prediction equations. Bull Seismol Soc Am 103:19–32

Stafford PJ, Mendis R, Bommer JJ (2008) Dependence of damping correction factors for response spectra on duration and numbers of cycles. ASCE J Struct Eng 134:1364–1373

Tolis SV, Faccioli E (1999) Displacement design spectra. J Earthq Eng 3:107–125

Trifunac MD, Lee VW (1989) Empirical models for scaling pseudo relative velocity spectra of strong earthquake accelerations in terms of magnitude, distance, site intensity and recording site conditions. Soil Dyn Earthq Eng 8:126–144

Walling M, Silva W, Abrahamson NA (2008) Nonlinear site amplification factors for constraining the NGA models. Earthq Spectra 24:243–255

Wu J, Hanson RD (1989) Study of inelastic spectra with high damping. J Struct Eng 115:1412–1431

Yenier E, Sandıkkaya MA, Akkar S (2010) Report on the fundamental features of the extended strong motion databank prepared for the SHARE project, p 44. Deliverable 4.1 of Seventh Framework Programme Project Seismic Hazard Harmonization in Europe (SHARE), 34 p, Ankara